AD-A210 499

Tracking Performance Evaluation

by

Shozo Mori
Kuo-Chu Chang
Chee-Yee Chong
Steve Spain

Prepared by
Advanced Decision Systems
Mountain View, California

Prepared for
MIT Lincoln Laboratory
Lexington, Massachusetts

7 December 1938

JUL 2 5 1989
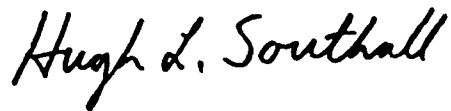
89 7 25 026

This technical report has been reviewed and is approved for publication.

FOR THE COMMANDER

Hugh L. Southall

Hugh L. Southall, Lt. Col., USAF
Chief, ESD Lincoln Laboratory Project Office

EXECUTIVE SUMMARY

This final report documents the results of the research conducted at *Advanced Decision Systems* (ADS) under a project entitled, "Discrimination Architecture Engineering Support," sponsored by *Lincoln Laboratory, Massachusetts Institute of Technology, MA.*, for the period from December 1, 1987 to August 31, 1988.

The research relates, in general, to performance evaluation of systems for tracking and classifying a large number of dense (closely-spaced) objects, and in particular, to tracking-surveillance and object-discrimination in a multi-layer ballistic missile defense system. The main purpose of the project is to identify a suitable set of *performance measures* and to develop simple *analytic models*. It is required that such models be capable of taking various problem parameters, such as

1. threat parameters, including threat trajectories and local densities,

2. sensor parameters, including sensor resolutions, measurement accuracies, detection probabilities, and false alarm rates,

3. other parameters, including geometrical relationships (viewing angles, sensor coverage, etc.), tracking time, number of frames, and sampling intervals

and converting them into a suitable tracking performance measure without performing extensive Monte-Carlo-type simulations.

It was decided that *track purity* is the most appropriate tracking performance measure mainly because it is a good measure for representing the quality of tracking outputs especially for object discrimination purposes. This measure would be important in many tracking situations where target classification is only possible after correlating data from different

time/sensor samples. Track purity (the percentage of correct measurements in a given track) can be decomposed into a series of performance evaluation of sequential correlation processes (e.g., track-to-measurement associations). Thus, a major part of the research efforts were devoted to establishing a simple analytic model for predicting the performance of single-scan track-to-measurement correlation. We have derived and validated the following *scaling law* for predicting the probability, P_C, of a track being associated with the correct measurement:

$$P_C = e^{-\pi\beta\bar{\sigma}^2} = e^{-\pi\bar{\beta}} = e^{-\bar{\nu}}$$

In this formula, the probability is expressed by the object density β on the sensor's focal plane and the average prediction error standard deviation $\bar{\sigma}$ (the error includes both tracking (i.e., prediction) error and sensor measurement error) or, equivalently, the object density $\bar{\beta}$ normalized by the error, or the expected number $\bar{\nu}$ of measurements in the one-σ area of the error ellipse.

In general, this simple expression models the performance of optimal solutions to the classical assignment problem in a probabilistic sense. The results of fairly extensive Monte-Carlo simulations showed that this law predicts the performance very well over a reasonably large range of assignment problems. We should note that this evaluation formula is *not* meant to be applied to any specific sensor system and/or tracking algorithms. Rather, it expresses a probabilistic upper bound on the association performance when only two parameters, i.e., object density and track prediction errors, are given. We have subsequently found out that an appropriate expression when false alarms are present is

$$P_C = e^{-\pi(\beta+2\beta_{FA})\bar{\sigma}^2}$$

where β_{FA} is the density of false alarms on the sensor's focal plane. This model was also verified by Monte-Carlo simulations.

With these basic models, a method for estimating average track purity given threat/sensor parameters was developed. The method depends on Cramér-Rao type bounds on the tracking accuracies and on dynamical models for predicting the object spatial densities. Again

the Cramér-Rao type bounds are used to obtain estimated upper bounds on tracking performance, thereby viewing potentially complicated tracking processes (e.g., track initiation, continuation, editing, elimination, multiple-hypothesis, etc.) as large black boxes and making the resultant expressions independent of any particular tracking algorithm. To verify the track purity prediction method we have developed, a small-scale simulation of ballistic object tracking with an orbiting sensor was conducted. More extensive tracking simulations or examination of performance of various tracking systems are planned for the next phase of this project.

Issues concerning limited sensor resolutions, i.e., *closely spaced objects*, were also investigated. Since our main object is to establish a method for estimating track purity, it is appropriate to view unresolved measurements as *bad* measurements (just as incorrectly associated ones). Thus, we have reduced the issues to a problem of predicting the frequencies of measurements being merged together, as functions of object densities on focal planes and sensor resolutions. We have developed a simple expression for the probability of an object being included into unresolved measurements. This simple expression was also tested by extensive Monte-Carlo simulations and found to be fairly accurate.

CONTENTS

LIST OF FIGURES

LIST OF TABLES

1. INTRODUCTION

This final technical report documents the results of the research which was conducted at *Advanced Decision Systems* (ADS) under a project entitled, "Discrimination Architecture Engineering Support," sponsored by *Lincoln Laboratory, Massachusetts Institute of Technology, MA*. The task is to develop an analytical model which relates scan-to-scan correlation performance to threat and sensor parameters. Since the emphasis is to to develop analytical methods for evaluating sensors' ability in tracking threat objects, the research effort at ADS is called "*Tracking Performance Evaluation.*"

1.1 Background

ADS' task is a part of Lincoln Laboratory's effort on Discrimination Architecture for the Sensors Directorate of SDI Office. This effort is concerned with modeling the interaction of different sensors operating together in various layers of a multi-layer ballistic missile defense system. A major element of such a system is a passive IR sensor operating in a track-while-scan mode and covering a large portion of the threat volume.

Such a system encounters various serious problems including:

- a large number of objects to be tracked and discriminated

- non-uniform distribution of object locations and velocities

- low observability – angle-only measurements (no range information)

- very high local object density compared with sensors' resolution

- nonlinear dynamics (ballistic trajectories) and nonlinear, time-varying observation (orbiting sensors)

- relatively long sensor revisit time compared with the time constant of object dynamics

There is a need to estimate the sensors' ability in tracking objects in this difficult tracking environment. For several reasons, it is desired to perform such estimation without

1

conducting simulations using detailed threat/sensor simulators and particular correlation algorithms. One of the reasons is to avoid expensive Monte Carlo runs. Other reasons include the desire to estimate the upper bound of the performance given basic threat/sensor parameters (independent of particular correlation algorithms), and to produce sensor parameter specifications to meet given tracking performance requirements.

Thus we need a simple analytic model relating scan-to-scan correlation performance as a function of threat and sensor parameters, which include:

- number of objects to be tracked and discriminated

- local spatial density of objects

- geometric relationship between threats and sensors, such as viewing angles, detection opportunities, etc.

- sensor resolution, measurement accuracy, detection probability and false alarm rate

- tracking time, number of frames, sensor revisit time, etc.

Since we may want to establish an upper bound on tracking performance, inclusion of operational parameters given to trackers (correlators), such as validation gate size (χ^2-value), various threshold values, etc., may or may not be desirable.

1.2 Objectives

ADS' task is to develop simple analytic models which relate correlation performance to key threat/sensor parameters. In particular, it is our goal to develop *scaling laws* to identify situations where similar performance can be expected and to permit rapid comparison of different scenarios to determine which will have better scan-to-scan correlation performance. In order to achieve this, it is necessary to develop simple measures of scan-to-scan correlation performance. Analytic models and scaling laws thus obtained must then be validated and, if necessary, calibrated through a series of small-scale simulations.

Figure 1-1 is a conceptual block diagram showing all the system components, and key functions and parameters. Our objective is to establish simple analytic models which relate

2

TRAJECTORY
PARAMETERS

GEOMETRY
RESOLUTION
DETECTION PROBABILITY
FALSE ALARM RATE
SAMPLING INTERVAL

VALIDATION GATE SIZE
TRACK/HYP. PRUNING THRESHOLD

TARGET
STATES

TARGETS

SENSORS AND
SIGNAL PROCESSORS

SCANS

TRACKER

TARGET STATE
ESTIMATES

TRACKING PERFORMANCE EVALUATOR

EVALUATION RESULTS
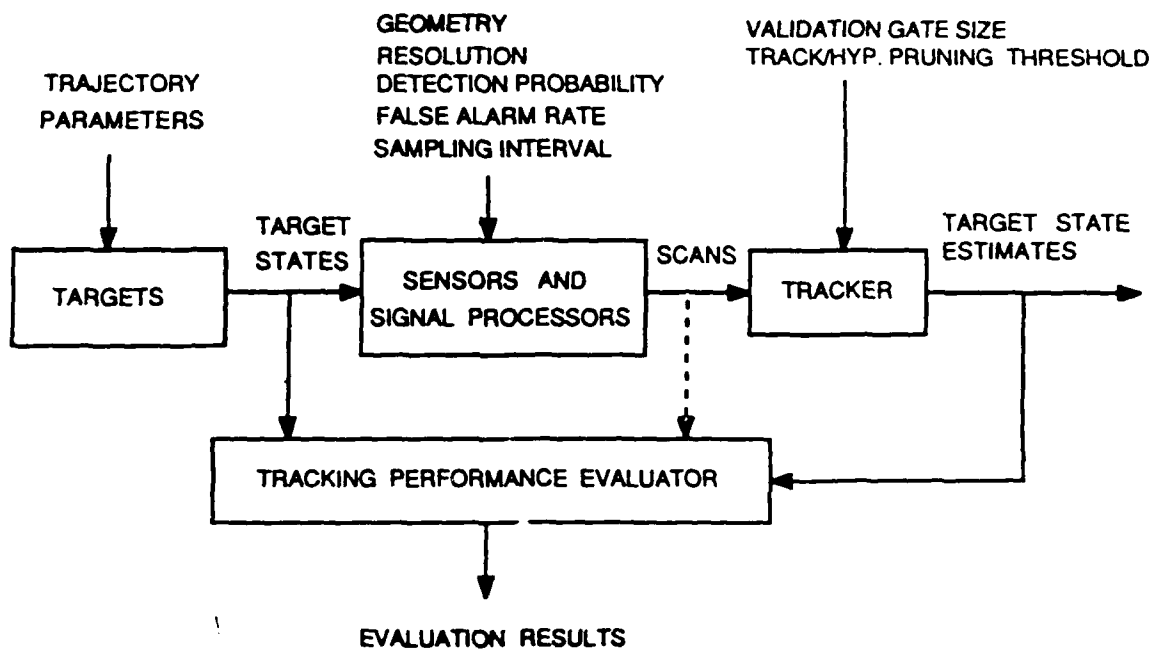
Figure 1-1: Tracking Performance Evaluation

3

all the input parameters, going into system components from above in Figure 1-1, to the tracking (correlation) performance metrics coming out at the bottom of the figure. One can view the whole system shown in Figure 1-1 as a system which detects objects and estimates their (six-dimensional) states. From this point of view, it is natural to consider performance metrics such as

- Percentage of missing objects (or fraction of objects which the system fails to track)

- Number of false (extraneous) tracks

- Tracking accuracy – six-dimensional state estimation errors

which are parallel to the standard set of performance evaluation metrics used for sensors, i.e., detection probability, false alarm rate and measurement accuracy. Unlike sensor signal processors which usually operate on a snap-shot (single-scan) basis, trackers or correlators involve very complicated data processing, and as a result, it is sometimes not straightforward as to how to define the above three metrics.

In our particular environment, i.e., in ballistic missile defense systems, however, it is more appropriate to measure the third criterion, i.e., tracking accuracy, as the closeness of the data-to-data correlation (partitioning of multi-scan detections) results to the real source of each measurement. This is so because, in the present stage of technology, effective object discrimination requires time series of measurements distinctively originating from each object to be discriminated. In other words, discrimination algorithms must rely on the correlation results of object trackers. In such a situation, mis-association generated by a tracker (correlator) is naturally a serious problem for a discrimination system, and it is very important to predict the magnitude of such mis-association. Thus our main objective is to predict tracking performance in terms of how pure each track is, in other words, how many mis-associations each track contains.

1.3 Technical Approach

As mentioned before, the primary objective of this research is to quantify the (potential) ability of tracking and discriminating objects given a set of threat/sensor parameters.

4

Therefore, it is desirable to conduct analysis independent of any specific tracking (correlation) algorithm. One way to accomplish this objective is to analytically evaluate the performance of the *optimal algorithm*. A class of general multi-target tracking problems has been formulated and optimal solutions to them have been developed. (See, e.g., [1]). Unfortunately, performance evaluation based on this general theory of multi-target tracking is extremely difficult even in Gauss-Poisson cases. This is so because such analysis cannot avoid complicated probabilistic calculation involving non-gaussian (typically χ^2) random variables. In fact, almost all the tracking algorithms (including the tracking algorithm specifically designed to solve the tracking problem in ballistic missile defense systems [2]) involve χ^2-type random variables in one way or another, which makes analytic evaluation very difficult.

Nonetheless, there have been a small number of papers and reports on this subject mainly considering specific algorithms, e.g., [3], [4] and [5]. Primary concerns were on statistics of *missing objects* and *false tracks*, and analytic results were obtained from Markov chain models which approximately describe detection history for each track. Therefore, emphasis was placed on *track initiation* performance rather than *track continuation*, and the possibility of mis-association was not considered. In the context of ballistic missile defense systems, or at least of in some phases of such systems, failure of track initiation or creation of (*permanent*) false tracks are not of central importance due to relatively high detection probability and substantially regular dynamics. Nonetheless, the track initiation itself is quite important due to the high object density, the limited resolution and the low observability (angle-only measurements). On the other hand, the track initiation problem may be made somewhat easier through system architecture concepts such as *birth-to-death* tracking. On the other hand, track quality in terms of track purity is of great importance for object discrimination and targeting purposes, and is thus the performance measure used in this study.

Since track purity may be expressed as a summation of the correctness of track-to-measurement correlation at each scan, the most critical analysis is that on the single-scan correlation performance. Our approach is first to establish a very simple analytic model which relates the single-scan correlation performance to a few parameters characterizing the scan in question, and then to relate that single-scan model to prediction of average track purity. Figure 1-2 summarizes our technical approach for this research. In order to develop

5
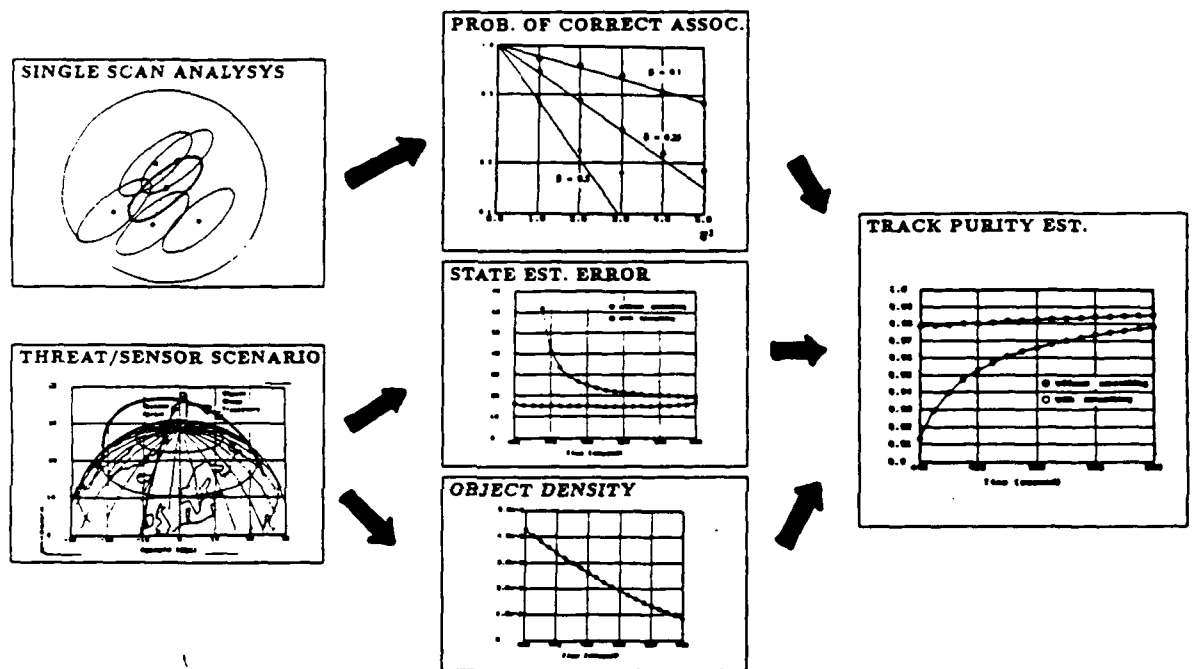
Figure 1-2: Technical Approach

a simple analytic model, we must base the single-scan analysis on a relatively simple mathematical model with several simplifying assumptions. However, crucial parameters must be adequately included. In our approach, the single-scan correlation performance is related to the measurement prediction accuracy by tracks and object density on the sensor's focal plane in each scan. These two key parameters can then be related to other parameters defined by threat/sensor scenarios. In arriving at analytic expressions for correlation performance, it is inevitable to simplify models by ignoring complicated factors and approximating mathematical formulae. In general, in our approach, initially analysis is conducted with many assumptions (sometimes restrictive), and then, relaxation of assumptions is attempted later one by one. Each step of analytic results will be verified as much as possible through Monte Carlo simulations.

The next section, Section 2, describes the single-scan correlation performance analysis which forms the basis of the majority of the results described in this report. The next section, Section 3, shows how key parameters used in Section 2 can be derived from a given threat/sensor scenario; this is followed by the expressions for track purity in Section 4. Throughout these sections, various kinds of Monte Carlo simulations are used to verify the analytic expressions. The last section, Section 5, summarizes the results and discusses directions for future research. Detailed mathematical derivations are presented in the Appendices.

2. SINGLE-SCAN ANALYSIS

This section describes the single-scan correlation analysis which serves as the basis of the studies presented in this report. In a sense, this section describes the problem of estimating track purity in its simplest form. Initially, we will ignore some factors, i.e., missed detections, resolution limitation (closely spaced objects), false alarms, etc. The effects of those factors will be considered later in this section or in the subsequent sections. The mathematical model used in this section is almost identical to that in [6], which analyzes the single-scan-based sensor-to-sensor correlation problem. The technical report [6], written fourteen years ago is concerned with the precise calculation of the probability of the most likely correlation being the correct one and draws its main results through the Fourier (characteristic function) technique. In this section, by introducing further simplifying assumptions, a very simple expression of the probability will be obtained as a basic scaling law.

2.1 Mathematical Model for Single-Scan Correlation Problem

Suppose that we have been tracking N objects in a number of scans from a sensor (or sensors) from which N tracks have been formed, and that there is a perfect one-to-one matching between the set of "real" objects and that of tracks. We assume, for the moment, there are neither false alarms nor missed detections in the previous scans as well as the scan to be considered here. Thus we consider a sensor scan consisting of N measurements, $y_1, ..., y_N$, with each y_i originating from the i-th object.[1] Assuming an angle-only measurement passive sensor, each y_i is modeled as a two-dimensional random vector,

$$y_i = z_i + n_i \qquad (2.1)$$

for each $i \in \{1, ..., N\}$, where z_i is the "true" projection of the position of the i-th object onto the sensor's focal plane and n_i is the additive zero-mean gaussian noise with a 2×2 variance matrix R_i.

---

[1] In an actual scan, it is natural to model the order of measurements as a realisation of a totally random (i.e., equally probable) permutation of a given object labeling. Here we are using the identity index map from the set of the objects to the set of measurements for notational convenience. For a correlator, the identity map is just one of all the equally probable permutations. See Appendix A for a related discussion.

On the other hand, for each $i \in \{1, ..., N\}$, the i-th track (tracking the i-th object) is associated with measurement prediction $\hat{y}_i$ which is modeled as

$$\hat{y}_i = z_i + m_i \qquad (2.2)$$

where m_i is a zero-mean gaussian random vector representing the measurement prediction error of the i-th track, with Q_i being its variance matrix.[2] We assume that the random vectors, $\hat{y}_1, ..., \hat{y}_N, n_1, ..., n_N, m_1, ..., m_N$, are independent from each other.[3]

In this simplified situation, it is natural to evaluate the performance of the optimal assignment algorithm. Each assignment is a permutation π on the index set $\{1, ..., N\}$, i.e., under a permutation π, the i-th track is assigned to the $\pi(i)$-th measurement. Under an appropriate set of assumptions, it can be shown[4] that an optimal track-to-measurement assignment is represented by a permutation which maximizes the assignment cost function

$$J(\pi) = \sum_{i=1}^{N} \chi(i, \pi(i))^2 \qquad (2.3)$$

over the set of all the permutations π on the set $\{1, .., N\}$, where, for each (i, j),

$$\chi(i, j) = \|\hat{y}_i - y_j\|_{S_{ij}^{-1}} \qquad (2.4)$$

with[5]

$$S_{ij} = Q_i + R_j \qquad (2.5)$$

which is assumed to be positive definite. Then the probability of the optimal assignment being the "true" one is the probability of the event in which $J(\iota) \leq J(\pi)$ for all the permutations π where ι is the identity map[6] representing the "true" assignment.

The problem of determining an optimal π to minimize (2.3) is the well-known classical assignment problem. It is also a well known result that, under a correct assignment ($\pi = \iota$),

---

[2] In an actual situation where ballistic objects are being tracked, each measurement prediction $\hat{y}_i$ and its associating error variance matrix Q_i are obtained by the nonlinear projection from the object state distribution for each track on to the sensor's focal plane.

[3] See Appendix A for discussions concerning this assumption.

[4] See Appendix A.

[5] By $\|z\|_A$, we mean a semi-norm of z in a Euclidean space defined by a nonnegative definite symmetric matrix A as $\|z\|_A \stackrel{\text{def}}{=} \sqrt{z^T A z}$. Thus, when I is the identity matrix, $\|z\| = \|z\|_I$ is the Euclidean norm of z. z^T is the transpose of a vector or matrix z.

[6] Namely, $\iota(i) = i$ for all $i \in \{1, .., N\}$

9

the assignment cost $J(\iota)$ is a χ^2 random variable with degree of freedom equal to N times the dimension (two) of the measurement space. It can also be shown that, when π is not a true association, $J(\pi)$ is a non-centric χ^2 random variable (See [6].). Although these results have been known among researchers for at least two decades, there is not much else in the form of analytical facts that we can point out.

2.2 Estimation of Probability of Correct Association

In [6], it was argued that the events in which three-way or more complex assignment errors happen in an optimal assignment are very rare so that we should only consider two-way mis-associations. This argument may be loosely supported by the following observation: Every permutation can be expressed as a composition of transpositions (two-way switches). Therefore, unless the probability of having each transposition is significantly high, two or more simultaneous transpositions involving the same object should not happen very often. It should be very rare particularly when the object density is not significantly high. For the moment, let us assume that transpositions are the only significant events.

Single Transposition: To simplify the discussion, let us consider each transposition independently, and thus, assume only two objects, i.e., $N = 2$. The event to consider is

$$E_{12} = \left\{ J(\{(1,1),(2,2)\}) \leq J(\{(1,2),(2,1)\}) \right\} \tag{2.6}$$

of two tracks being correctly associated with measurements. As seen in [6] and in Appendix B, the calculation of this probability is not easy and evaluation may be possible only through numerical methods, e.g., Fourier transformation (i.e., by evaluating the characteristic function of a non-centric χ^2 random variable), which will not lead to any analytic expression useful for our purpose. However, when we assume $Q_1 = Q_2$ and $R_1 = R_2$, and when conditioned by the predictions by tracks, we have a simple probabilistic expression,

$$\text{Prob}(E_{12}|\hat{y}_1, \hat{y}_2) = \text{erf}\left(\frac{1}{\sqrt{2}} \|\hat{y}_1 - \hat{y}_2\|_{S^{-1}} \right) \tag{2.7}$$

where[7]

$$S_{ij} \equiv S \tag{2.8}$$

---

[7]$\text{erf}(\cdot)$ is the error function defined as $\text{erf}(z) = \frac{1}{\sqrt{2\pi}} \int_{-\infty}^{z} e^{-\xi^2/2} d\xi$.

10
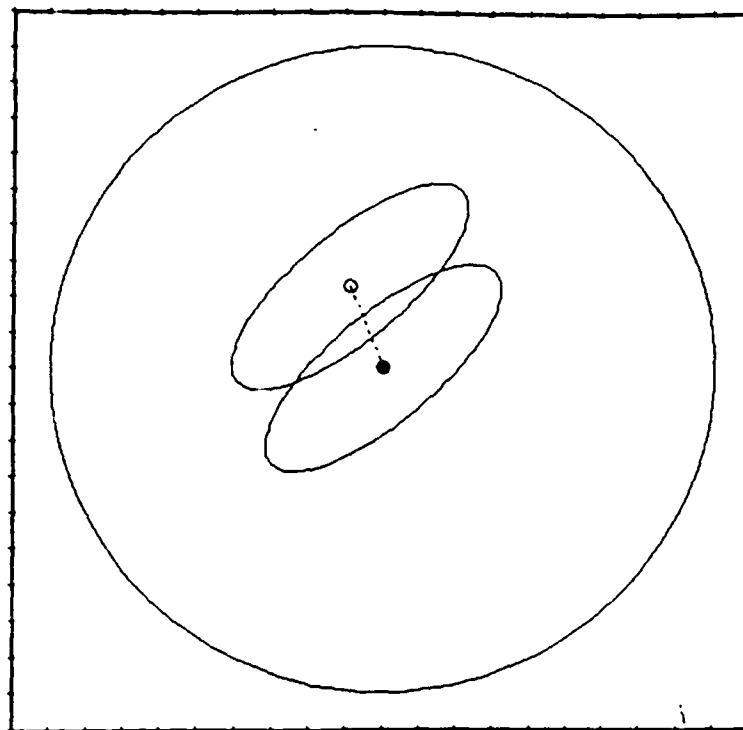
Figure 2-1: Single-Scan Analysis: Two Objects

for all $(i,j) \in \{1,2\} \times \{1,2\}$. This assumption, (2.8), may be justified in situations where object states in a group are very similar and so are the SNR's of each detection. It may not be a very plausible assumption, however, in special situations, e.g., when two object groups are crossing or merging on a sensor's focal plane. Even in such situations, with enough number of frames being accumulated, this assumption may become eventually a close approximation of the reality.

Assume further that $\hat{y}_1 - \hat{y}_2$ is distributed uniformly on a disk with radius r, or equivalently that $\hat{y}_1$ is at the origin 0 and $\hat{y}_2$ is distributed uniformly on the disk with radius r (See Figure 2-1.). Define an *average prediction error standard deviation* $\bar{\sigma}$ as the geometric average of the semi-major and the semi-minor of the ellipse defined by $\|y\|_{S^{-1}} = 1$, i.e.[8],

$$\bar{\sigma} = [\det(S)]^{1/4} \qquad (2.9)$$

Then, as shown in Appendix B, when the radius r is large enough compared with the square root of maximum eigenvalue, i.e., the semi-major of the ellipse defined by S, the unconditional

---

[8]By $\det(A)$, we mean the determinant of a square matrix A.

11
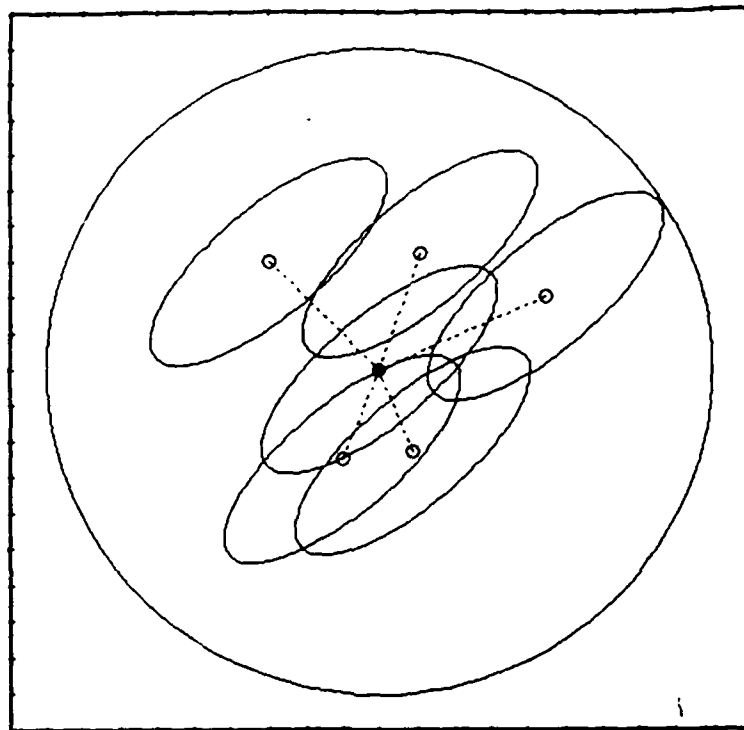
Figure 2-2: Single-Scan Analysis: N Objects

probability of the event E_{12} can be expressed simply as

$$\text{Prob.}(E_{12}) \approx 1 - \left(\frac{\bar{\sigma}}{r}\right)^2 a \tag{2.10}$$

Multiple Transpositions: Now let us go back to our N-object model. Without loss of generality, we can place the track we are concerned with, say the first track, at the origin, i.e., $\hat{y}_1 = 0$. Assume that all the other tracks are uniformly distributed on the disk with radius r (See Figure 2-2). This assumption should not be too restrictive as far as the radius r is large enough compared with the average prediction error standard deviation $\bar{\sigma}$ and the track we are considering, i.e., $\hat{y}_1$, is not almost on the edge of the track group's extent. Furthermore, let us assume (2.8) for all pairs (i, j) of indices for tracks and measurements. Let E_c be the event in which there is no transposition between the first track $\hat{y}_1$ and any of the remaining tracks. Then, by assuming that any mis-association is caused by one or more such transpositions involving the first track, the probability of the first track being correctly associated with the measurement can be simply expressed (following from (2.10)) as

$$\text{Prob.}(E_c) \approx (\text{Prob.}(E_{12}))^{N-1} \approx \left(1 - \left(\frac{\bar{\sigma}}{r}\right)^2\right)^{N-1} \approx 1 - \pi\beta\bar{\sigma}^2 \tag{2.11}$$

12

where β is the object density on the focal plane, i.e.,

$$\beta = \frac{N-1}{\pi r^2} \approx \frac{N}{\pi r^2} \qquad (2.12)$$

assuming $N \gg 1$.

It follows from (2.11) that, when the number N of objects is a random integer with a Poisson distribution, the probability of the track being associated with the correct measurement becomes

$$\text{Prob.}(E_c) \approx \exp\left(-\pi\beta\bar{\sigma}^2\right) \qquad (2.13)$$

where the object density β is now re-defined as

$$\beta = \frac{\nu}{\pi r^2} \qquad (2.14)$$

with ν being the expectation of the number N of objects, which is now re-defined as a Poisson random variable.

The expression (2.13) is the most important result in the studies described in this report. It is a simple scaling law which expresses the probability of correct association as the function of 1) object density β on the focal plane and 2) the average measurement prediction error standard deviation $\bar{\sigma}$. Since (2.13) is a function of $\beta\bar{\sigma}^2$, we can have a simpler expression

$$\text{Prob.}(E_c) \approx \exp(-\pi\bar{\beta}) \qquad (2.15)$$

where $\bar{\beta}$ is the normalized object density defined by

$$\bar{\beta} = \beta\bar{\sigma}^2 = \beta\sqrt{\det(S)} \qquad (2.16)$$

It should be noted that (2.15) claims that the correlation performance is determined solely by the normalized object density (defined by (2.16)) on the focal plane.

Monte Carlo Simulation: To verify the scaling law (2.13) or (2.15), a series of Monte Carlo simulations were performed. Figure 2-3 shows the results. For each run, a hundred tracks were simulated by generating $(\hat{y}_i)_{i=1}^{100}$ uniformly on a disk with an appropriate size, and then one hundred measurements, $(y_i)_{i=1}^{100}$, were generated according to eqns. (2.1) and (2.2). Then the optimal assignment was calculated by Munkres algorithm ([7]), and it is subsequently compared with the true track-to-measurement correspondence. The probability

13
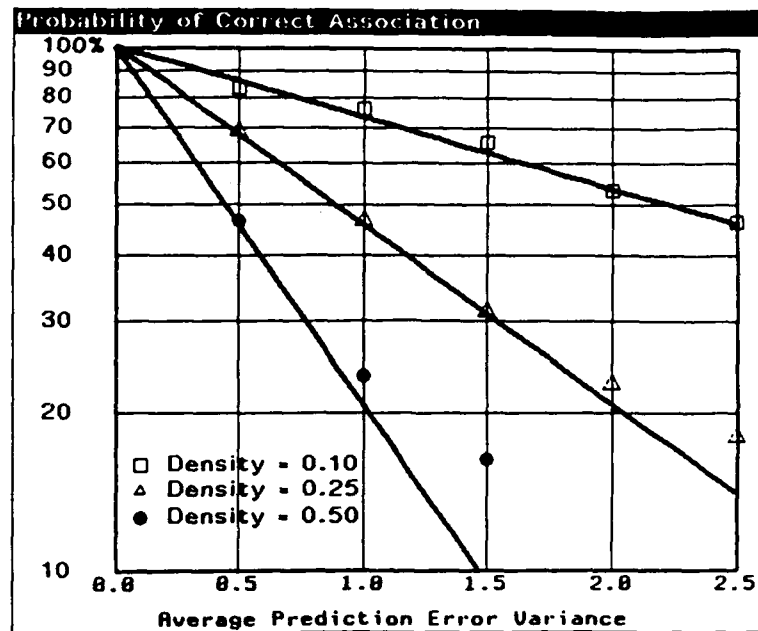
Figure 2-3: Single-Scan Correlation Performance (1)

of correct association is defined as the percentage of tracks which were correctly assigned with measurements and is averaged over 50 samples for each point in Figure 2-3. The measurement prediction error variance matrix S was chosen to be a diagonal matrix with the same diagonal elements. The cases with non-diagonal matrices, or in other words, the non-zero eccentricity of the ellipse defined by $\|y\|_{S^{-1}} = 1$, will be discussed later in Section 2.3.

When we derived the scaling law, (2.13), we used a mathematical model which places the track to be considered at the origin and assumed other tracks are distributed uniformly around it. When a track is situated at the peripheral of a track group, the track density which affects the probability of correct association effectively decreases. This kind of "edge" effect was not considered in (2.13). Since the purpose of the Monte Carlo simulation is to verify the appropriateness of the simple mathematical expression (2.13), we considered only the tracks which are within a disk with half the radius of that of the disk over which all the tracks are uniformly distributed, thereby eliminating the edge effects. We will discuss issues concerning uneven object density later in this section.

14
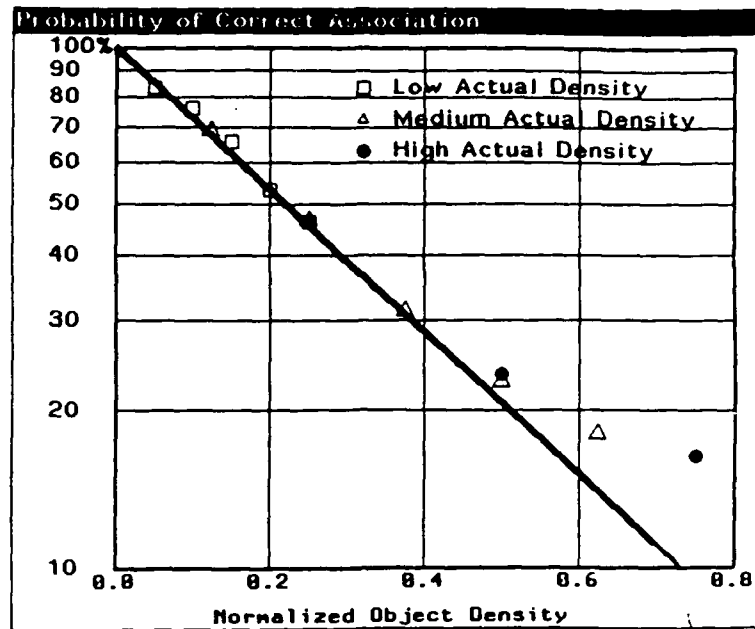
Figure 2-4: Single-Scan Correlation Performance (2)

Figure 2-3 shows the results with three different object densities, i.e., β being .1, .25 and .5 objects per unit area (distinguished by three different symbols in the figure), as plots of the correct association probability versus the average measurement prediction variance $\bar{\sigma}^2$ (measured by unit area), together with the scaling law (2.13). Figure 2-4 plots the same data using the normalized object density defined by (2.16) and compares them with the scaling law (2.15). Figure 2-4 uses the same symbols used in Figure 2-3 for different actual (not normalized) object densities. In Figures 2-3 and 2-4, the empirical results agree with our analytic results, eqns. (2.13) and (2.15), very well except for regions where we have high object densities or large measurement prediction errors. In such regions, however, both actual and predicted correlation performance are very bad, i.e., with probability of correct association being 50% or less, and hence, it is not reasonable even to try track-to-measurement correlation at all. Nonetheless, it is interesting to see that the actual optimal assignment performs much better than the theoretically expected performance. This deviation seems to originate from the fact that, in our analysis, the mis-association mechanism is modeled simply by composition of independent transpositions, and complicated multiple-way mis-associations

15
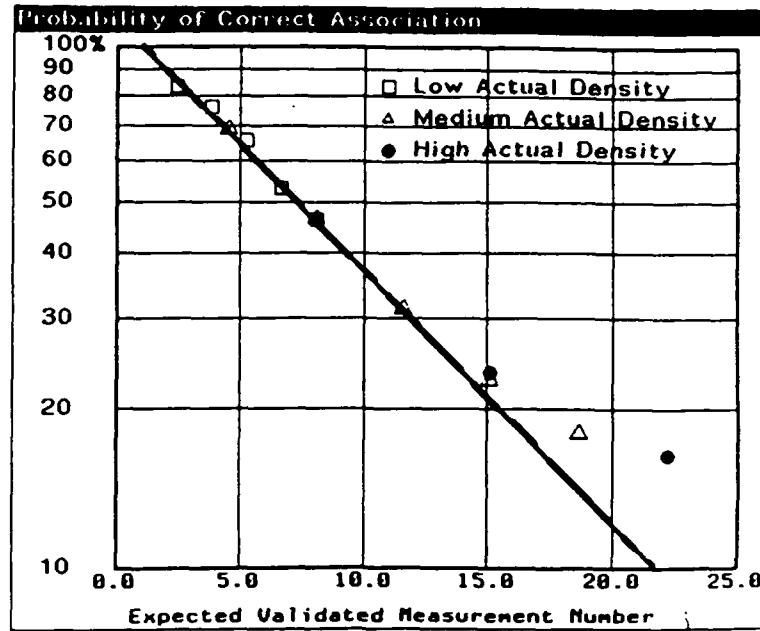
Figure 2-5: Single-Scan Correlation Performance (3)

and dependence of association errors (ignored in the analysis) cannot be ignored in high object density or large measurement prediction error cases. Another explanation for this deviation is simply the increase of "edge" effects which we have discussed before. (See also Appendix B for related discussions.) Figure 2-5 shows the same plots as those in Figure 2-4 but the abscissa is taken as the expected number of measurements in the validation gate of each track. The expected number ν_G of measurements per track validation gate is calculated as

$$\nu_G = 1 + \pi\beta\chi_G^2\sqrt{\det(S)} \tag{2.17}$$

where χ_G^2 is the χ^2-value to determine the validation gate size. In this plot, the value, $\chi_G = 3$, is used.

It may be interesting to see that, in actual simulations, how often multiple switches, i.e., mis-association not caused by simple transpositions, happen. Table 2-1 shows the average number of occurrence of various kinds of mis-associations with different normalized object densities, $\bar{\beta}$ (using unit $1/\pi$). As seen in the table, the occurrence of complicated object switches increases as the object density increases. However, within the range where

16

Table 2-1: Mis-Association Statistics

$\beta(1/\pi)$	Two-Way Switches	Three-Way Switches	Four Ways or More
.02	.7	0	0
.05	1.9	.1	0
.1	3.8	.4	.1
.2	6	1.2	.1
.5	9	2.8	1.4
1	10.1	4.7	4.6
2	7.2	3.6	6.8

the probability of correct association is meaningful, say about 50 %, the two-way switches dominates more complicated switches. This is consistent with the fact that the scaling law, (2.13) or (2.15), considering only two-way switches, predicts the assignment performance relatively well (as seen in Figures 2-3 through 2-5). The effects of complicated switches which are not modeled in our analysis are not clear. The fact that the simple expression, (2.13) or (2.15), fits well with simulation results indicates overall cancellation of over-estimation of the performance with under-estimation.

2.3 Effects of Eccentricity of Error Ellipse

In the single-scan analysis in this section, we have assumed the prediction error variance matrices, S_{ij}, for all the track-measurement pairs are identically equal to a matrix S. The matrix S (which is assumed to be positive definite) defines an ellipse[9], $\{y \in \mathcal{R}^2 | \|y\|_{S^{-1}}^2 = 1\}$. In the simulations, the results of which are shown in the previous section, 2.2, we have assumed zero eccentricity. In this subsection, we will examine the effects of eccentricity of the error ellipses and measure such effects by means of Monte Carlo simulations to confirm the validity of our analytic expression, i.e., (2.13). According to (2.13) together with the definition (2.9) of the average error standard deviation $\bar{\sigma}$, the probability of correct association can be expressed as

$$\text{Prob.}(E_c) \approx \exp(-\beta A)$$

---

[9] $\mathcal{R} = (-\infty, \infty) = $ set of real numbers.
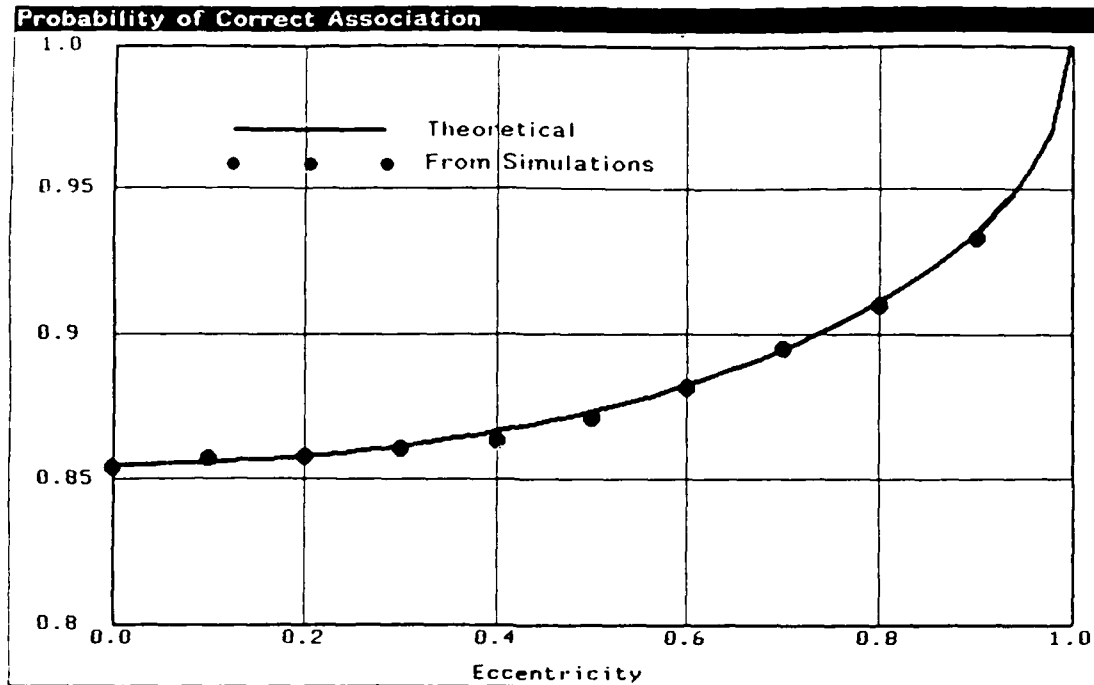
Figure 2-6: Effects of Eccentricity of Prediction Error Ellipses

where A is the area of the error ellipse defined by $\{y \in \mathcal{R}^2 | \|y\|_{S^{-1}}^2 = 1\}$. In other words, the probability of correct association can be expressed as

$$\text{Prob.}(E_c) \approx \exp\left(\text{Expected Number of Objects in Error Ellipse}\right)$$

Let μ_1 and μ_2 be the two (strictly positive) eigen-values of the matrix S, and let $a = \max\{\sqrt{\mu_1}, \sqrt{\mu_2}\}$ and $b = \min\{\sqrt{\mu_1}, \sqrt{\mu_2}\}$ be the semi-major and the semi-minor of the ellipse. Then the average prediction error standard deviation $\bar{\sigma}$ defined by (2.9) can be rewritten as

$$\bar{\sigma} = a\sqrt{1 - e^2} \tag{2.18}$$

and hence, (2.13) becomes

$$\text{Prob.}(E_c) \approx \exp(-\pi\beta a^2(1 - e^2)) \tag{2.19}$$

where e is the eccentricity of the ellipse.

Figure 2-6 shows the probability of correct association where the semi-major a of the error ellipses and the object density β are fixed such that

$$\tilde{\beta} = \beta\bar{\sigma}^2 = \beta a^2 = .05$$

18

when the eccentricity is zero ($e = 0$) and the eccentricity is varied from 0 to 1. This figure also shows the results of Monte Carlo simulations. For each Monte Carlo simulation point shown in the figure, 200 samples are taken for the simulation using 100 objects. As seen in the figure, the simulation results closely follow the theoretical curve shown by the solid curve.

2.4 Uneven Local Object Density

In Section 2.2, we have derived simple scaling laws to determine the probability of correct association as a function of object density and track measurement prediction errors. To do so, we have assumed objects are distributed uniformly on a given region of the sensor's focal plane. This uniformity assumption may not validly reflect reality. For example, if objects are distributed uniformly within a ball in a three-dimensional space, apparently their projections onto a plane are not distributed uniformly. In general, the two-dimensional projection of a group of three-dimensional objects is such that object density is in general a decreasing function of the distance from the center of the image. As will be shown in Section 4, even in such a case, if the object density is appropriately calculated, the scaling law, (2.13) or (2.15), still provides us with relatively accurate performance prediction. However, one may want to question how uneven local object density affects the correlation performance, in particular, one may want to quantify the difference in correlation performance between inner objects and outer ones, within the same object group.

A naïve way to derive an expression which may handle the dependency on the varying object density would be

$$\text{Prob.}(E_c) \approx \exp\left(-\pi\beta(\rho)\tilde{\sigma}^2\right) \tag{2.20}$$

or

$$\text{Prob.}(E_c) \approx \exp(-\pi\bar{\beta}(\rho)) \tag{2.21}$$

which are obtained directly from (2.13) and (2.15) (resp.) by simply replacing the constant object density β (normalized density $\bar{\beta}$) by non-constant density, e.g., the density, $\beta(\rho)$ or $\bar{\beta}(\rho)$, depending on the distance ρ from the center of the track group. However, there is no immediate justification to do so. This is so because, although we can model varying object

19
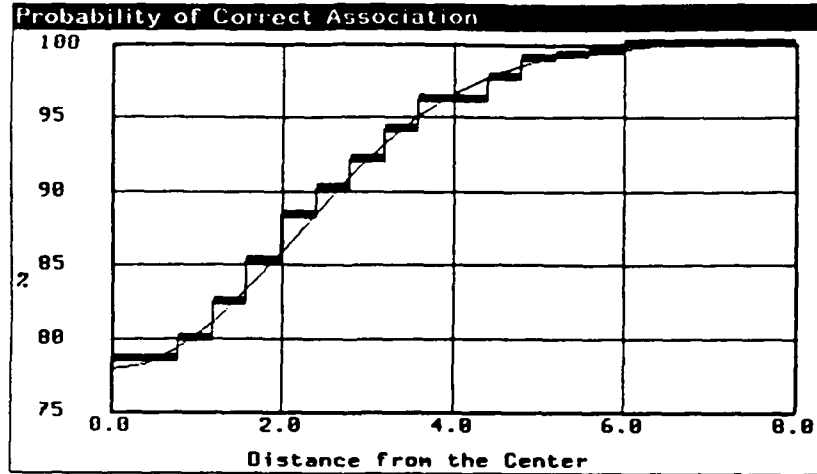
Figure 2-7: Uneven Probability of Correct Association

density by a non-constant function β or $\bar{\beta}$, such notion is only valid for a small region where we cannot ignore the extent of the prediction error ellipse. Nonetheless, when the object density is a monotonic (decreasing) function of the distance from the center, the effects of the slope of the object density may be averaged out so that expression (2.20) or (2.21) is in fact a good approximation for the non-uniform local object density.

In order to illustrate this point, the probability of correct association was calculated assuming a gaussian density, i.e.,

$$\beta(\rho) = \frac{\nu}{2\pi\Sigma^2}\exp\left(-\frac{1}{2}\left(\frac{\rho}{\Sigma}\right)^2\right) \tag{2.22}$$

with $\Sigma \gg \bar{\sigma}$, where ρ is the distance from the center of a track group and ν is the expected total number of tracks in the group, rather than assuming a uniform density. Appendix C shows (2.20) is in fact a good approximate expression in such a case. This analysis is also supported by a Monte Carlo simulation, the results of which are show in Figure 2-7. The curve shown in this figure is obtained from (2.20) and (2.22) with $\nu = 20$, $\Sigma = 2$ and $\bar{\sigma} = .2$. This theoretical curve is supported by a Monte Carlo simulation whose results are

20

shown in the figure by step functions. The simulation produces 300 samples of a 20-object scenario according to (2.22) with parameters consistent with the curve. Then all the correct associations and mis-associations are sorted according to the distance of the track from the center of the group, and the average probability of correct association is calculated for each interval of the distance. The figure shows that the simulation results coincide with the theoretical curve surprisingly well, suggesting that this kind of "gaussian" model may be used to investigate the unevenness within an object group in terms of correlation performance.

2.5 Effects of False Alarms

In section 2.2, we have derived a very simple but relatively accurate expression for the probability of correct association by first 1) calculating the probability of transposition (two-way switch) of objects (assuming only two objects) and then 2) identifying the event of correct association as the one in which no transposition takes place with any of the surrounding objects. With this approach, it is rather straightforward to take false alarms into account. Recalling that E_c is the event of a track being associated with a correct measurement, let E_{ct} be the event that there is no transposition between the track in question and any other surrounding track and E_{cf} be the event that there is no transposition between the track and any of the false alarms which surrounds it. Then we have

$$\text{Prob.}(E_c) = \text{Prob.}(E_{ct})\text{Prob.}(E_{cf}) \tag{2.23}$$

which may be supported by the assumption that tracks (i.e., objects) are independent of false alarms.

For the sake of simplicity, let us assume that the common prediction error variance matrix S is an identical matrix with the same diagonal element $\bar{\sigma}^2$. Then as shown in Appendix D, we have

$$\text{Prob.}(E_{ct}) \approx \exp(-\pi\beta\bar{\sigma}^2) = \exp(-\pi\bar{\beta}) \tag{2.24}$$

and

$$\text{Prob.}(E_{cf}) \approx \exp(-2\pi\beta_{FA}\bar{\sigma}^2) \tag{2.25}$$

where β_{FA} is the density of false alarms. It is interesting to observe that the two expressions (2.24) and (2.25) are almost identical with the difference of the factor 2, which originates

21
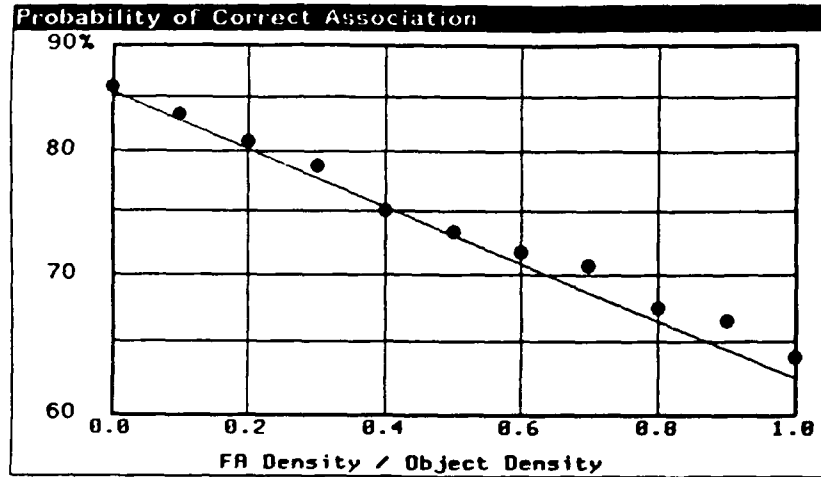
Figure 2-8: Effects of False Alarms

from the fact that measurements from other tracks contain their prediction errors while false alarms are simply assumed to distributed uniformly around the track in question.

It follows from (2.23), (2.24) and (2.25) that

$$\text{Prob.}(E_c) \approx \exp(-\pi(\beta + 2\beta_{FA})\bar{\sigma}^2) = \exp(-\pi\beta(1 + 2\gamma_{FA})\bar{\sigma}^2) = \exp(-\pi\bar{\beta}(1 + 2\gamma_{FA})) \quad (2.26)$$

where γ_{FA} is the ratio of the false alarm density over the object density on the focal plane, i.e., β_{FA}/β. Figure 2-8 shows the effects of the false alarms on the probability of correct association. In this figure, the theoretical curve defined by (2.26) is shown as well as Monte Carlo simulation results (shown by dots). The normalized object density $\bar{\beta}$ of .1 is used for this figure and the ratio of the false alarm density over the object density is chosen as the independent parameter. For the simulation, 100 targets are generated for each run and each point is obtained form 50 samples. As seen in this figure, simulation results support the simple expression (2.26). As observed in Figure 2-3 and Figure 2-4, the theoretical expressions give us slightly pessimistic predictions when the correlation performance is degraded substantially due to dense false alarms.

22

2.6 Summary of Section 2

In this section, we have presented the major results of the studies described in this report, i.e., the scaling law expressed by (2.13) and (2.15). This analytical expression is very simple and yet we have shown, by means of extensive Monte Carlo simulations, that it may provide very accurate prediction for single-scan correlation performance. A crucial assumption in deriving this expression is that the prediction error variance matrix S_{ij} for each track-measurement pair is (at least almost) identical, which may be valid when we track a group of objects whose state vectors are close together. Issues concerning the shape of the error ellipses, the uneven local object density and the false alarms, have been also discussed in this section. Issues concerning the unresolved measurements (i.e., closely spaced objects) will be included in Section 4.

3. TRACK ACCURACY AND OBJECT DENSITY

In Section 2, we have developed a very simple scaling law which predicts the single-scan correlation performance as a function of object density on the focal plane and the average prediction error standard deviation. These two variables are time-varying and depend on threat/sensor scenarios. In this section, we will discuss how to obtain these two variables from a given set of scenario variables, together with other related issues.

3.1 Cramér-Rao Type Bound

This sub-section discusses how to obtain the average prediction error standard deviation $\bar{\sigma}$ defined by (2.9). The standard deviation $\bar{\sigma}$ is determined by the prediction error variance matrix S which we are assuming (at least approximately) identical for every track-measurement pair. In Section 2, we have modeled the prediction error by an additive gaussian random vector as in (2.2). For an actual track, the measurement prediction $\hat{y}$ and the variance matrix S are calculated from the six-dimensional state estimate and its error variance prediction associated with the track. Unless all the past measurement associations are given, it is impossible to calculate or estimate the state estimation errors. To keep the development simple, we will first consider a track with perfect past measurement association, which will give us a form of upper bound on the correlation performance for a given scan. The effects of the past data mis-associations will be discussed later.

When all the data associations are known, estimation of the six-dimensional state of a ballistic object becomes a well-defined continuous-time dynamics discrete-time measurement filtering problem. Due to the non-linearity, there is no analytic way of accurately predicting the filtering performance. Fortunately, it is possible to calculate a Cramér-Rao type lower bound on the state estimation errors using a method similar to the one used in [8]. The technique can be well summarized by the following quotation from the reference [9]:

> "....... the extended Kalman filter variance propagation equations *linearized about the true unknown trajectory* provides the Cramé-Rao lower bound to the estimation error variance matrix."

In other words, we can solve the Riccati-type differential equation using partial derivatives about the true trajectory to obtain a lower bound on the state estimation error variance matrix, from which we can calculate a lower bound on the measurement prediction error variances.

Consider a track which consists of a set of measurements at different times indexed as $\{t_k\}$ (in general from multiple sensors) and assume that the object being tracked is governed by the ballistic dynamical equation

$$\frac{d}{dt}x(t) = f(x(t)) \tag{3.1}$$

where $x(t)$ is the six-dimensional state consisting of the 3-dimensional position and velocity, and f is the gradient of the potential due to the earth's gravity. The track contains the measurement at each time t_k as

$$y_k = h(x(t_k), t_k) + w_k \tag{3.2}$$

with white gaussian noise sequence $\{w_k\}$. The function $h(\cdot, t_k)$ projects the three-dimensional object position onto the sensor's focal plane at time t_k.

For the sake of simplicity, assume that there is no *a priori* information. Then the lower bound P_k on the state estimation (filtering) error variance matrix at time t_k can be written as

$$P_k^{-1} = \sum_{i=1}^{k} \Psi(t_k, t_i)^T H_i^T R_i^{-1} H_i \Psi(t_k, t_i) \tag{3.3}$$

where $\Psi(\cdot, \cdot)$ is the fundamental solution matrix satisfying

$$\frac{\partial}{\partial t}\Psi(t, s) = -\Psi(t, s)\frac{\partial f}{\partial x}(x(t)) \tag{3.4}$$

with the boundary condition $\Psi(s, s) = I$ where I is the six-dimensional identity matrix. H_k in (3.3) is the matrix of the observation partial about the true state at time t_k, i.e.,

$$H_k = \frac{\partial h}{\partial x}(x(t_k), t_k) \tag{3.5}$$

and R_k is the measurement error variance matrix for the n-th observation. Finally the measurement prediction error variance matrix for the scan at time t_k is calculated as

$$S_k = H_k P_k H_k^T + R_k \tag{3.6}$$

25

Table 3-1: Choice of State Space for Cramér-Rao Bound Calculation

State Space	Dynamics	Observation
Cartesian	Simple Nonlinear	Simple Nonlinear
Range, Az, El	Complicated Nonlinear	Linear
Orbital Elem.	Linear	Complicated Nonlinear

In the above equations, (3.1) - (3.6), we have assumed that the object state is expressed in the six-dimensional cartesian coordinates with the origin at the center of the earth. However, the results (3.6) should remain the same even when we use a different coordinate system. Table 3-1 shows the possible choices of the coordinate system for the state space. Appendix E describes the forms of functions, (f, h), in each coordinate system. One of our objectives is to calculate the performance estimates quickly given a small set of necessary threat/sensor parameters. The choice of the coordinate system may be related to this requirement. Nonetheless, we did not find any particular difficulty in solving the differential equations, (3.1) and (3.4), in the standard six-dimensional cartesian coordinate.

As a preliminary investigation, we assume a simple scenario assuming a threat consisting of a group of ballistic objects and a single orbiting sensor. Figure 3-1 illustrates the threat and the sensor trajectories. The two circles in the figure indicate the centroid of the threat and the sensor position at a given time. The threat trajectory is a minimum-energy trajectory and the sensor orbit is a low-altitude circular one. This example was constructed so that the threat is visible from the sensor for most of the threat trajectory. Figure 3-2 shows the results of calculations of the average prediction error standard deviations $\bar{\sigma}$ assuming perfect data association at each scan. This figure shows the average prediction error standard deviations calculated by (2.9) and normalized by a constant sensor measurement error standard deviation with three different sampling intervals, 5, 10 and 20 seconds. Each curve shown in the figure has a peak around time 350 sec. when the distance from the sensor to the threat group is at a minimum so that the prediction errors are magnified, and exhibits a pseudo-stationary behavior just before and after this peak.

As seen in Figure 3-2, when a track has only a few scans of data, the prediction errors are very big, partially because of the low observability of the angle-only measurements by the
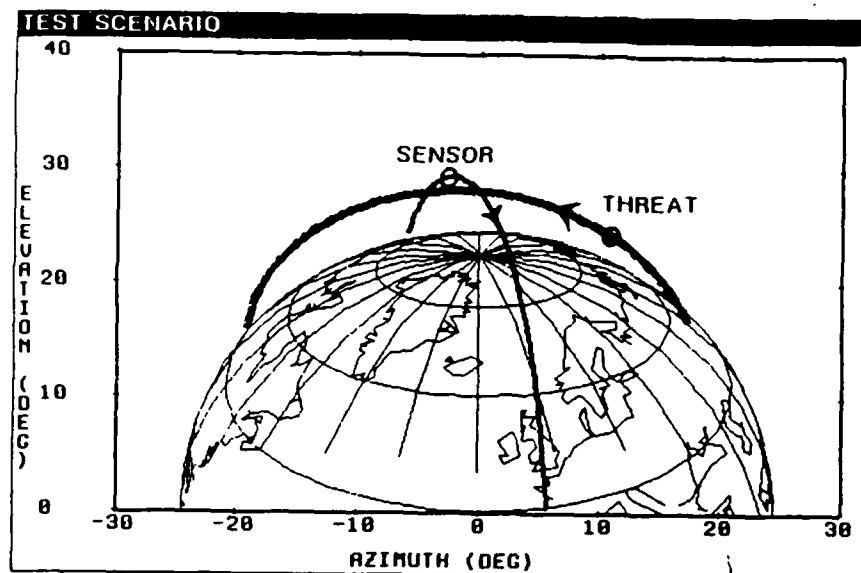
26

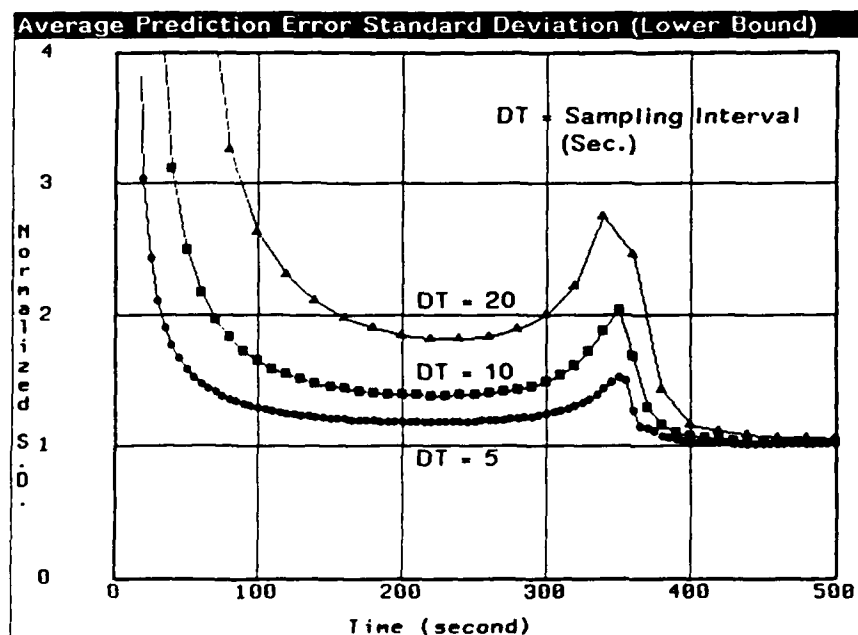Figure 3-1: Test Case Threat/Sensor Scenario

Figure 3-2: Average Prediction Error Standard Deviation

27

sensor. This poor prediction performance by tracks will result in very poor correlation results if a simple correlation algorithm discussed in Section 2 were used; in fact, correlation results from such an algorithm may be so bad as to become meaningless. Generally, the problem of generating meaningful tracks under such conditions is referred to as the *track initiation problem*. Many techniques have been developed, including the general multi-hypothesis technique described in [1]. Several techniques were developed specifically for ballistic missile defense systems (with which we are concerned in this report), i.e., [10], [11] and its refinement.

From the view-point of track purity, tracks in this track initiation phase may be too poor to be useful for the user we have in mind for this report, i.e., an object discrimination system. Hence we may consider a track initiation period as a time interval to produce *a priori* information to tracks and consider only subsequent intervals for object discrimination, which is more or less consistent with the underlying assumptions made in our analysis described in this report.

Under some conditions, however, it is desirable to provide as many data as possible for object discrimination and even to include the measurements in the initiation phase. In such a situation, it is reasonable to "re-do" the data-to-data correlation after tracks accumulate enough measurements to establish "good" state estimates. One simple way of viewing such a process is to consider track-to-measurement correlation using the *smoothing state estimates* rather than the *filtering state estimates* as indicated by (3.3). A lower bound on the estimation error variance for the smoothing state estimate can be obtained by simply replacing the range of summation in (3.3) by a larger interval, e.g., up to a given K as

$$\bar{P}_k^{-1} = \sum_{i=1}^{K} \Psi(t_k, t_i)^T H_i^T R_i^{-1} H_i \Psi(t_k, t_i) \tag{3.7}$$

Correspondingly we may replace P_k in (3.6) by $\bar{P}_k$. Figure 3-3 shows an example comparing the "filtering" predictions with the "smoothed" predictions. However, it is not very clear if the use of the smoothing estimation error variances in this way can be justifiable (or useful) or not. For example, it is not clear if we should use the "smoothed" state estimation error variance to predict performance of such "delayed" correlation since the information in the measurements are already included in the "smoothed" state estimate.

28

Average Prediction Error Standard Deviation
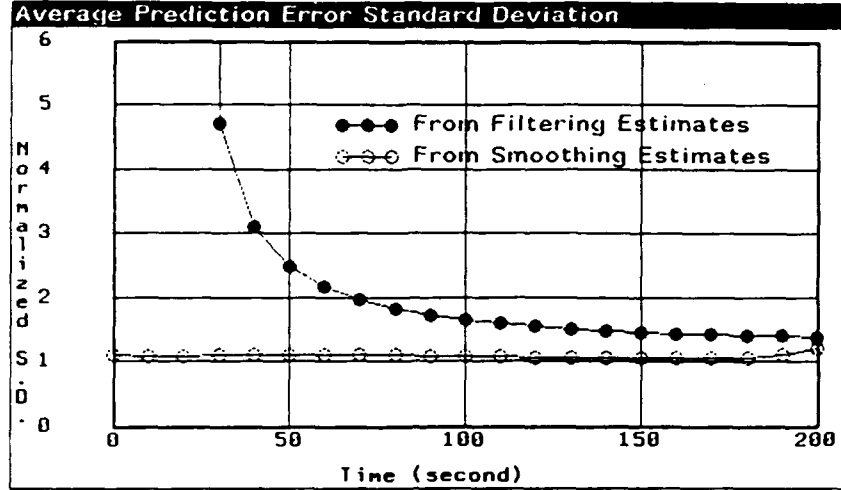
Figure 3-3: Average Prediction Error Standard Deviation - Smoothed -

3.2 Object Density Estimation

This sub-section discusses the calculation of the other parameter needed for the simple scaling law, (2.13) or (2.15), i.e., the object density β on the sensor's focal plane. We will seek a simple analytic method to calculate this quantity from a given set of threat parameters.

Consider N ballistic objects and let $x_i(t)$ be the 6D state of the i-th object at time t. When all the objects are separated (no interaction among them) and the only force applied is the earth's gravitational force, all the states $x_i(t)$ obey the same differential equation, $\dot{x}_i = f(x_i)$. Let us define the centroid by

$$\bar{x}(t) \stackrel{\text{def}}{=} \frac{1}{N} \sum_{i=1}^{N} x_i(t) \tag{3.8}$$

and the spatial variance by

$$V(t) \stackrel{\text{def}}{=} \frac{1}{N} \sum_{i=1}^{N} (x_i(t) - \bar{x}(t))(x_i(t) - \bar{x}(t))^T \tag{3.9}$$

29

Then, if the distance $\|x_i(t) - \bar{x}(t)\|$ of each object state from the centroid is small enough, the centroid and the variance follow the extrapolation equations

$$
\begin{aligned}
\frac{d}{dt}\bar{x}(t) &= \frac{1}{N}\sum_{i=1}^{N}\frac{d}{dt}x_i(t) \\
&= \frac{1}{N}\sum_{i=1}^{N}f(x_i(t)) \\
&\approx \frac{1}{N}\sum_{i=1}^{N}\left(f(\bar{x}(t)) + \frac{\partial f}{\partial x}(\bar{x}(t))(x_i(t) - \bar{x}(t))\right) \\
&= f(\bar{x}(t))
\end{aligned}
\tag{3.10}
$$

and

$$
\begin{aligned}
\frac{d}{dt}V(t) &= \frac{d}{dt}\left(\frac{1}{N}\sum_{i=1}^{N}x_i(t)x_i(t)^T - \bar{x}(t)\bar{x}(t)^T\right) \\
&\approx \frac{1}{N}\sum_{i=1}^{N}\left(\frac{\partial f}{\partial x}(\bar{x}(t))(x_i(t) - \bar{x}(t))x_i(t)^T + x_i(t)(x_i(t) - \bar{x}(t))^T\frac{\partial f}{\partial x}(\bar{x}(t))^T\right) \\
&= \frac{\partial f}{\partial x}(\bar{x}(t))V(t) + V(t)\frac{\partial f}{\partial x}(\bar{x}(t))^T
\end{aligned}
\tag{3.11}
$$

The spatial variance $\Sigma(t)$ on a sensor's focal plane at time t can then be approximated as

$$
\Sigma(t) \approx \frac{\partial h}{\partial x}(\bar{x}(t), t)V(t)\frac{\partial h}{\partial x}(\bar{x}(t), t)^T
\tag{3.12}
$$

where $h(\cdot, t)$ is the function which maps a point in the six-dimensional state space to a two-dimensional angular measurement at time t on the focal plane of a given sensor. The object density on the focal plane can be calculated as a ratio of the total number of objects over the area of the elliptic region defined by the variance matrix $\Sigma(t)$, using an appropriate χ^2 value, as

$$
\beta(t) = \frac{N}{\pi\chi^2\sqrt{\det(\Sigma(t))}}
\tag{3.13}
$$

Figure 3-4 shows an example object density on a sensor's focal plane as a function of time. The scenario used for this calculation is the same as the one used in the last section. The initial spatial variance has been more or less randomly chosen. The χ^2 value corresponding to the 99%-inclusion probability was used for (3.13). The object density in the figure is normalized by the sensor's measurement error standard deviation. The dip of the curve in Figure 3-4 corresponds to the point where the distance between the threat group

30
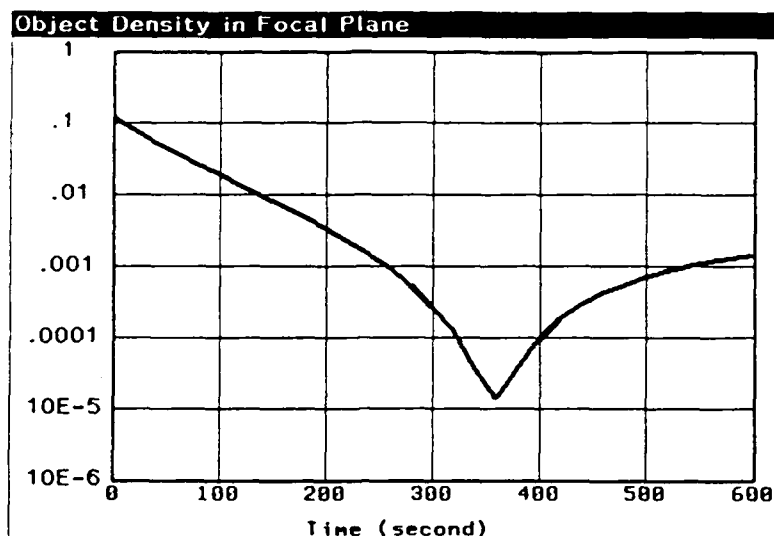
Figure 3-4: Object Density on Sensor's Focal Plane

and the sensor is at a minimum. As seen in this figure, unlike the prediction error variance, in general, there is no apparent "stationary" behavior. The initial condition for (3.12) was set to be

$$
V(t_0) = \begin{bmatrix} 0 & & 0 & \\ & \sigma_v^2 & 0 & 0 \\ 0 & 0 & \sigma_v^2 & 0 \\ & 0 & 0 & \sigma_v^2 \end{bmatrix} \tag{3.14}
$$

with a given σ_v which we can relate to as the *dispersion rate* of a threat object group. Needless to say, the χ^2 value in (3.13) is sensitive to the calculation of the object density β and an appropriate value is yet to be investigated.

3.3 Effects of Mis-Association

Mis-association for a track in a scan may create significant measurement prediction errors in the subsequent scans. Such errors may be characterized as *estimation bias* in the sense that the estimates may be further away from the "true" values than being indicated by the variance matrices accompanying the estimates. Apparently, the effects of mis-association

31

will be propagated from scan to scan. They may be magnified or be corrected in later scans. For example, a mis-association in one scan produces a bias which makes mis-associations in the subsequent scans more likely. On the other hand, if the track happens to be associated with the true measurement in the next scan, the bias may be compensated and the measurement predictions may recover for the subsequent scans. Thus the mechanism in which the effects of mis-associations are propagated from scan to scan is very complicated, and hence, very hard to model. Recently it was proposed ([13]) to extend Markov-chain modeling techniques used for estimating track initiation probability (e.g., in [3], [4], [5]) to model such a mechanism.

We tried to incorporate this Markov-chain-model technique into our framework, but no significant results were obtained. Difficulties lies in specifying the necessary transition probabilities necessary for building the Markov-chain model to describe the propagation of mis-association effects. From a limited number of simulations using a Markov-chain model, we tentatively concluded that the effects of mis-associations may not be very significant in a dense target environment. This may be so because even when a mis-association happens the "wrong measurement" must be *close enough to be mistaken* so that the effects may fall within the range of sensor measurement errors. On the other hand, if the object density as well as false alarm density is substantially low, the probability of having mis-association should be very low. Thus there may be an intermediate range of object density where the effects of mis-association may significantly affect the tracking performance.

3.4 Parameterization of Threat/Sensor Geometry

In the calculation of the average prediction error standard deviation $\bar{\sigma}$ and the object density β, we have utilized all the parameters defining the orbits of the threat centroid and the sensor. In order to have a simple expression, it may be desirable to parameterize the geometric relationship between the threat and the sensor orbital parameters. In situations where time constants in threat/sensor dynamics are substantially longer than those in our environment, we may consider parameters such as *range, aspect angle, depression angle, relative velocity,* etc. However, as seen in the previous figures in this section, the geometric relation may never be stationary. When a particular sensor has a period of blockage, either

32

due to the earth field-of-view blockage or the loss of SNR for threats appearing on the earth's surface, parameterization becomes even more difficult.

At this point, it is not clear at all if we may be able to do any meaningful parameterization or not. As indicated in Section 3.1., use of a special coordinate system for threat/sensor orbital elements may provide some insight on this problem.

4. TRACK PURITY ESTIMATION

In previous sections, we have established a method for predicting the single-scan data association performance given a set of threat/sensor parameters. In this section, the prediction of track purity based on the single-scan performance predictions will be discussed. We will also discuss the issues concerning unresolved measurements (CSO's).

4.1 Definition and Prediction of Track Purity

As in Section 3.1, let us consider sensor scans (in general from multiple sensors) indexed by time t_k. Suppose that we are given a set K of scan indices and that we wish to define the *purity* of a given track. For example, K is a set of scan indices for several consecutive scans from one of the sensors used in a tracking system. It is natural to define the purity as

$$\text{Track Purity} = \frac{\text{No. of scans with correct measurement assignments}}{\text{Total no. of scans in } K} \tag{4.1}$$

An immediate problem with this definition is the treatment of unresolved (merged) measurements and mis-detections. The problem of limited sensor resolution will be discussed in the next two sections. On the other hand, it is not quite clear even how to treat failed detections. If an object is not detected but associated with a measurement, it is clearly a mis-association. But if it is correctly recognized (as undetected), it is not clear if we should count it as a "correct association" or not. In this report, by assuming that the detection probability is high enough, it was decided not to include mis-detections in the discussion of track purity.

The purpose of this section is to produce a reasonable prediction on the *average track purity* given threat/sensor parameters. For this purpose, consider a *fictitious* binary stochastic process $\{m_k\}$ with discrete index k in the set K. The event, $m_k = 1$, represents a track-measurement mis-association, i.e.,

$$\text{Prob.}\{m_k = 0\} = P_C(\beta_k, \bar{\sigma}_k) = \exp(-\pi\beta_k\bar{\sigma}_k^2) \tag{4.2}$$

where $P_C(\beta_k, \bar{\sigma}_k)$ is the (average) probability of a track being correctly associated with a measurement at the scan k as a function of the object density β_k and the average prediction

34

error standard variation $\bar{\sigma}_k$. In fact, the function P_C is the scaling law described by (2.13) in Section 2.2. The total number of mis-associations in a given set of scans is then simply

$$\mathbf{M}[K] = \sum_{k \in K} \mathbf{m}_k \tag{4.3}$$

We may view the track purity defined by (4.1) for each track as a sample of the random variable[1], $\mathbf{M}[K]/\#(K)$, and hence, calculate the *average track purity* as

$$\mu[K] = \frac{1}{\#(K)} \sum_{k \in K} P_C(\beta_k, \bar{\sigma}_k) \tag{4.4}$$

When $\max_k \{1 - P_C(\beta_k, \bar{\sigma}_k)\}$ is small enough, we may apply the *law of small numbers* (See, e.g., [14]) and show that we may approximate the distribution of the random variable $\mathbf{M}[K]$ by a Poisson distribution with the mean

$$\nu[k] = \sum_{k \in K} (1 - P_C(\beta_k \bar{\sigma}_k)) \tag{4.5}$$

4.2 Treatment and Prediction of Unresolved Measurements (CSO's)

The first question we must answer concerning unresolved measurements (CSO's) is how we should count such measurements in calculating the track purity. When we view tracking as a state estimation problem with multiple objects, we may consider a correlation result as *correct* if a track is associated with an unresolved measurement with multiple origins one of which is the "true" origin of the track. In general, an unresolved measurement contains a *bias* when it is considered as a measurement for a given track, thereby somewhat discounting the "correctness" of the association.

As mentioned before, the primary concern of this report is the track purity seen from an object discrimination system. When two or more objects create a single detection, it is generally extremely difficult to separate out the contribution for each separate object from the merged detection. At least, this is not clear when examining a functional model developed for simulation purposes ([15]). If indeed it is not possible to extract useful information for object discrimination from unresolved measurements, then it is appropriate to count the unresolved measurements as *impure* measurements which are as *bad* as *mistaken* measurements. When

---

[1]By $\#(A)$, we mean the cardinality, i.e., the number of elements, of a set A.
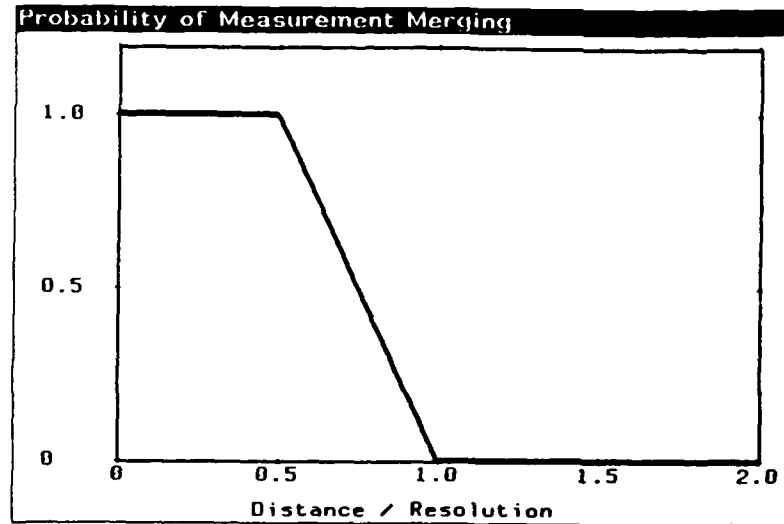
Figure 4-1: Probability of Measurement Merging (1)

we taking this point of view, we should simply discount the track purity by the probability
of the detection (corresponding to a track in question) being unresolved.

We will base our calculation of the probability of measurements being unresolved on the
functional model described in [15]. Consider two objects represented by two two-dimensional
vectors, y_1 and y_2. According to [15], the probability of measurements from these two objects
being unresolved can be modeled by a function p_m of the distance $d = \|y_1 - y_2\|$ between
the two objects. A good model for p_m is

$$p_m(d) = \begin{cases} 1 & \text{if} \quad 0 \leq d \leq \delta/2 \\ 2\dfrac{\delta - d}{\delta} & \text{else if} \quad \delta/2 < d < \delta \\ 0 & \text{otherwise} \end{cases} \qquad (4.6)$$

which is shown in Figure 4-1, where δ is the sensor resolution. With this model and a set of
assumptions, we can show (See Appendix F.) that an appropriate expression of track purity
considering unresolved measurements is

$$\mu[K] = \frac{1}{\#(K)} \sum_{k \in K} P_C(\beta_k, \bar{\sigma}_k)(1 - P_M(\beta_k)) \qquad (4.7)$$

36
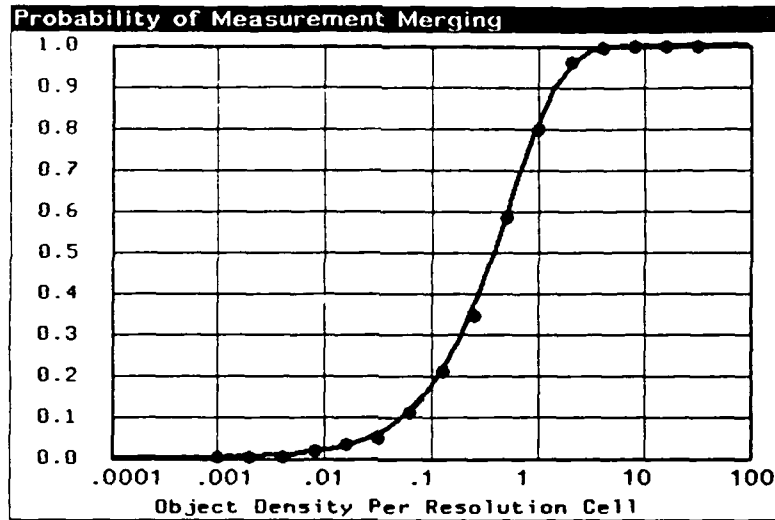
Figure 4-2: Probability of Measurement Merging (2)

where $P_M(\beta_k)$ is the probability of a track merged with another track and is expressed as

$$P_M(\beta_k) = 1 - \frac{2}{\delta\sqrt{\beta_k}}\left(\text{erf}\left(\sqrt{2\pi\beta_k}\delta\right) - \text{erf}\left(\sqrt{2\pi\beta_k}\frac{\delta}{2}\right)\right) \tag{4.8}$$

with δ being the sensor resolution. (See Appendix F for the derivation.)

Figure 4-2 shows the measurement merging probability P_M as a function of object density. The curve in the figure is the plot of (4.8) while each point (small filled circle) is obtained by 500-run Monte Carlo simulations with 100 simulated objects for each run. In the figure the object density is normalized by the sensor resolution cell area, i.e., δ^2. As seen in this figure, the expression (4.8) provides us with an accurate estimate on the probability. Figure 4-3 shows the probability of correct association using different object density values and the deterioration of the performance due to the unresolved measurements. In this figure, one curve (broken) represents the expression ignoring the CSO's, i.e., (4.4), and the other (solid) the one considering them, i.e., (4.7). Each point in the figure is the actual correlation performance obtained by simulations with unresolved measurements. In the simulations, a functional model described in [15] was used. This functional model takes the deterioration

37

Probability of Correct Association

Expected Prob. w/o CSO
Expected Prob. w CSO
Simulated Results

Normalized Target Density
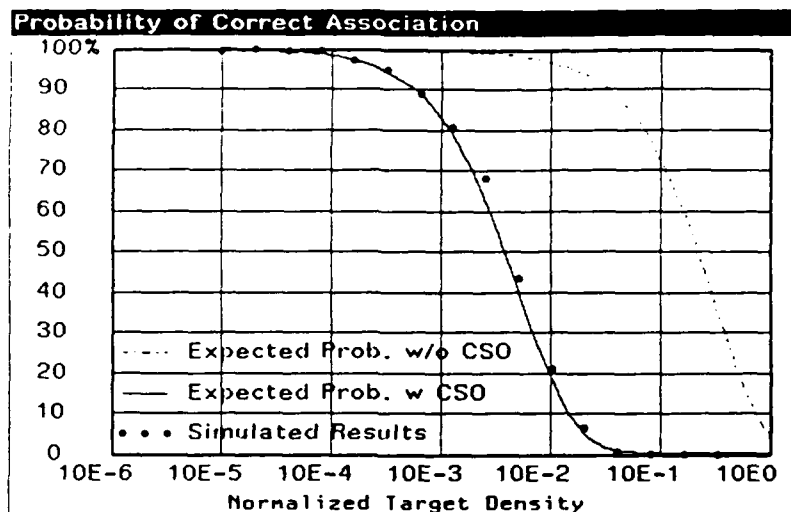
Figure 4-3: Probability of Correct Association

of measurement accuracy due to neighboring measurements into account. As seen in this figure, (4.7) accurately predicts the correlation performance with unresolved measurements.

4.3 Simulation Results

The test scenario of Figure 3-1, consisting of a threat object group and an orbiting sensor, was used to compare the analytic prediction of the average track purity with simulated tracking results. A simple tracking algorithm was used for this purpose. In particular, track initiation problems were avoided by using relatively "good" *a priori* information.

The tracking algorithm may be summarized as follows:

1. For each scan, first the object state distributions of all the existing tracks are extrapolated to the time of the scan, and then measurement predictions are made for each track using the sensor position at the time.

2. Then, for each existing track, an association list consisting with potential measurements and the track-measurement association χ^2 values is created.

38

3. Munkres algorithm is then used to obtain the optimal assignment in terms of track-measurement pairs.

4. The tracks which are not assigned to any measurement are then examined. For each of such tracks, if a measurement is found such that the χ^2 value is within a given threshold, the track-measurement pair is added to the assignment list made in the above step. (This step is to account for tracks which have been resolved in the past scans but not resolved in the current scan.)

5. The object state distributions of all the tracks included in the assignment list are then updated by the assigned measurements.

6. All the measurements which are not assigned to any track are then examined. For each of such measurements, a track for which the χ^2 value is minimized is then searched. If the minimal χ^2 value is within a given threshold value, then the track is split using this measurement.

7. The remaining measurements are then examined as potential sources to initiate tracks together with the *a priori* object state distribution attributed to the threat group with a simple thresholding scheme.

8. Then all the tracks are checked and, according to a simple rule, redundant or "bad" tracks are eliminated.

We have conducted two simulations; one with all the measurements being resolved and the other one with unresolved measurements, to clarify the effects of CSO's. Unfortunately, due to time and other resource constraints, only a single sample run for each case was conducted, and hence, we cannot conclude the validity of our analytic models beyond sample variations.

The parameters used in the scenario are the same as the ones described in Section 3.1. Figure 4-4 shows the estimated average track purity calculated according to (4.4) (i.e., without considering unresolved measurements) for three different sampling intervals, 5, 10 and 20 seconds. Figure 4-5 shows the Cramér-Rao type lower bound on the prediction error
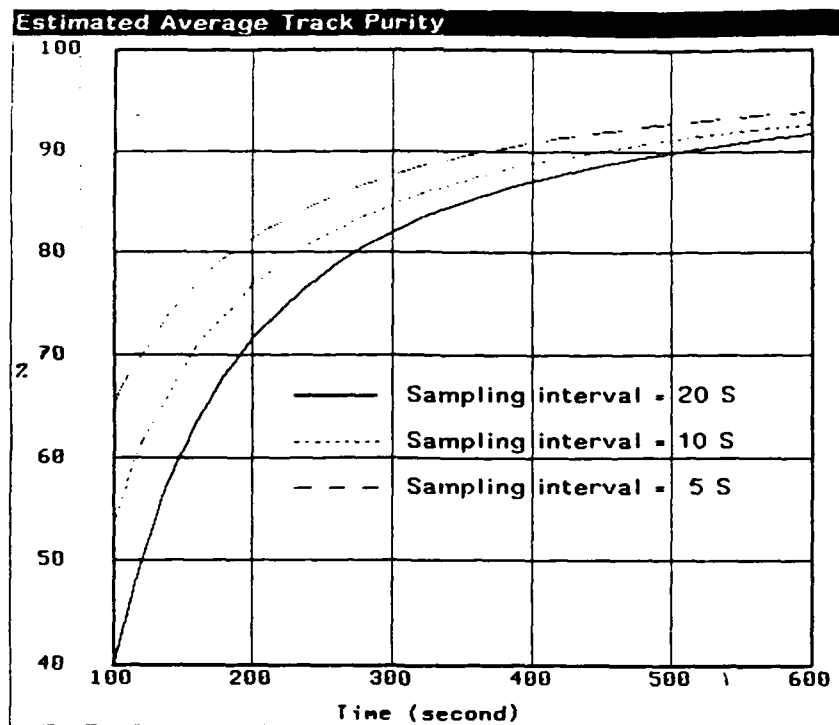
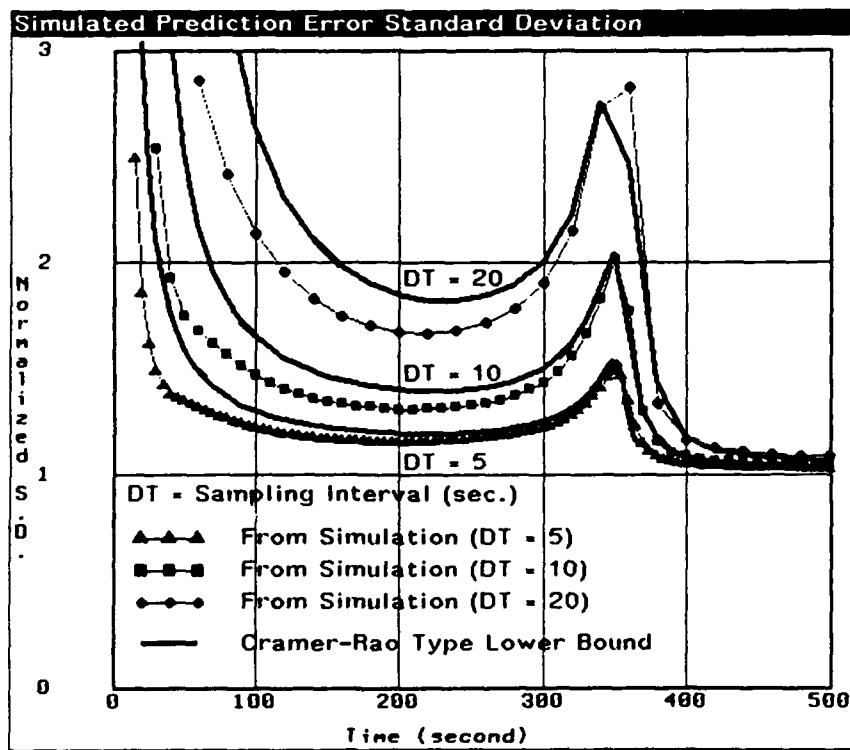Figure 4-4: Estimated Average Track Purity As a Function of Time (1)

Figure 4-5: Prediction Error Standard Deviation (Simulated Data)

40

Average Track Purity (Estimated vs Simulated)

Legend:
- Expected Purity (20 S)
- Simulation Results (20 S)
- Expected Purity (10 S)
- Simulation Results (10 S)
- Expected Purity (5 S)
- Simulation Results (5 S)

x-axis: Time (second), range 400 to 600
y-axis: 80 to 100, with 90 marked (z 90)
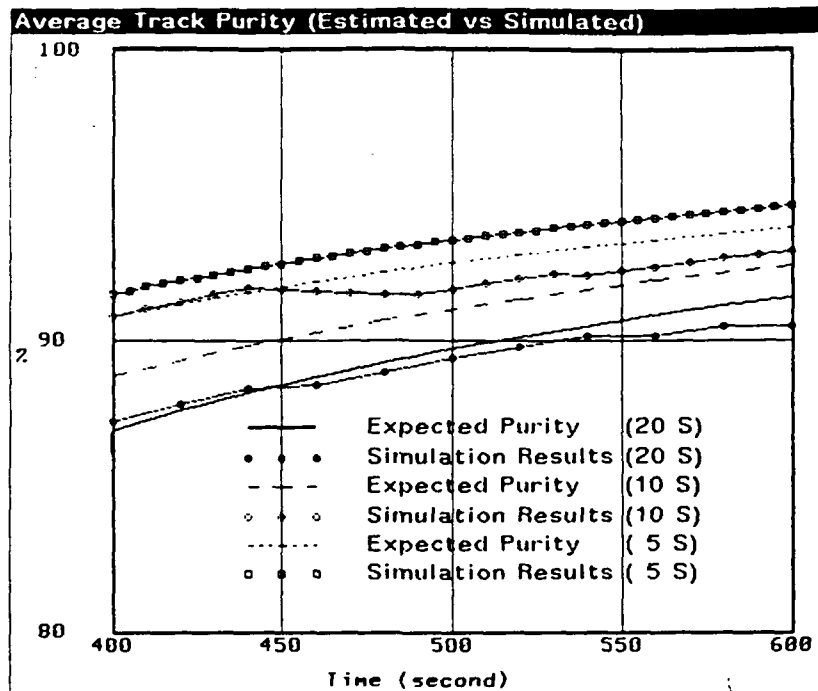
Figure 4-6: Average Track Purity (Estimated vs Simulated) (1)

standard deviations (used to calculate the curves in Figure 4-4). Figure 4-5 also plots the average prediction error standard deviations calculated from actual tracks in the simulation. The "lower bounds" in Figure 4-5 are greater than the actual standard deviations. This is so because the lower bounds were calculated assuming that no *a priori* information is available. Thus the differences between the analytic curves and the actual averages (from the simulation) show the effects of the *a priori* information we have assumed in the simulation. Figure 4-6 shows the comparison of the average track purity predicted by our analysis with the one obtained from the simulation, with three different sampling intervals. Some persistent difference between the analytic results and simulation results is seen in this figure. As mentioned before, however, the simulation results are only from one sample run, and hence, it may not be possible to draw any definite conclusion from these results, except for the fact that the simulation results are generally close to our analytically predicted curves.

In the simulations (using three different sampling intervals and the results of which are shown in Figures 4-4 to 4-6), all the measurements are resolved and, assuming a constant SNR, a fixed sensor measurement error variance was assumed. Another simulation

41

Probability of Measurement Merging
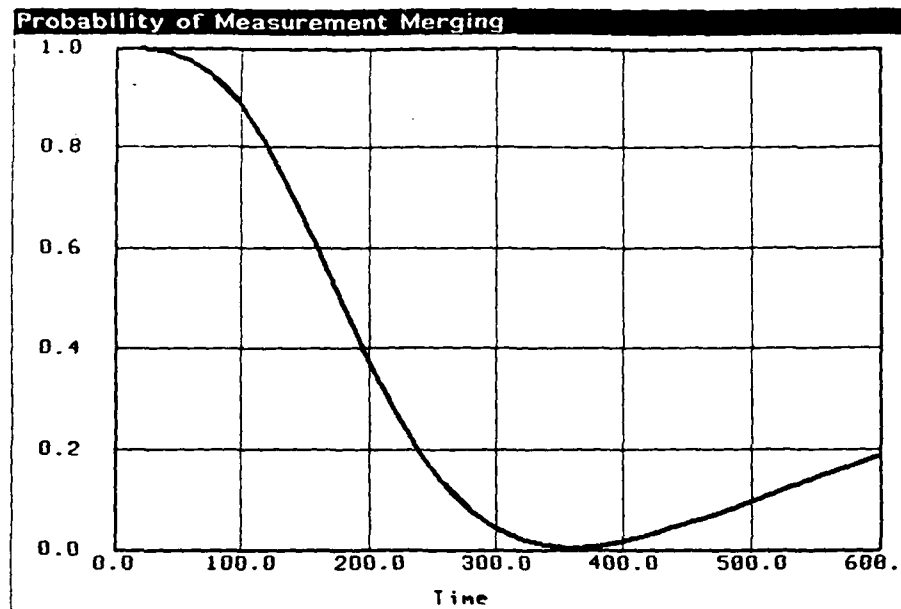
Figure 4-7: Probability of Measurement Merging As a Function of Time

was conducted with unresolved measurements. The functional model described in [15] was used for sensor measurement simulation assuming a constant SNR. First, the probability of measurement merging was calculated as a function of time, using (4.8). The results are shown in Figure 4-7. A dip of the curve in the figure corresponds to the time when the distance between the threat group and the sensor is minimum and so is the object density. Figure 4-8 shows two average track purity curves as functions of time, which are predicted from our analysis; one with unresolved measurements and the other assuming all the measurements are resolved. The difference between the two curves is due to the probability of measurement merging shown in Figure 4-7. Figure 4-9 compares the track purity predicted (4.7) (considering the unresolved measurements as "impure measurements") with the results from a simulation run. Although there is some initial disagreement between the two results, in general, the predicted track purity is very closed to that obtained from the simulation, ESPECIALLY as the number of scans is accumulated, . When evaluating the simulation results, all the past measurement assignments of each track at various stage are examined and the majority of the origins of the past measurements is then used for the "true" origin of

42

Figure 4-8: Estimated Average Track Purity As a Function of Time (2)

Figure 4-9: Average Track Purity (Estimated vs Simulated) (1)

43

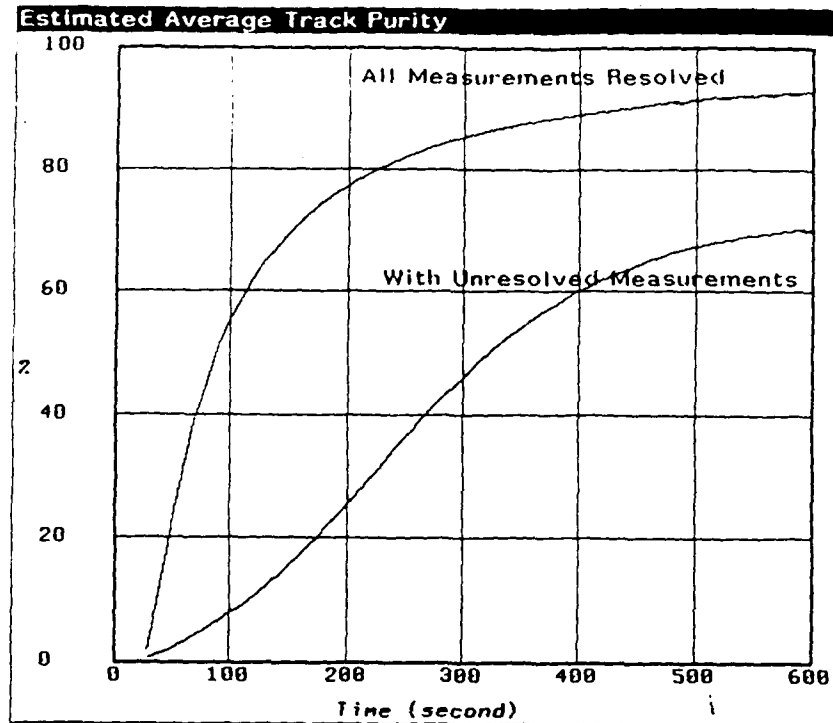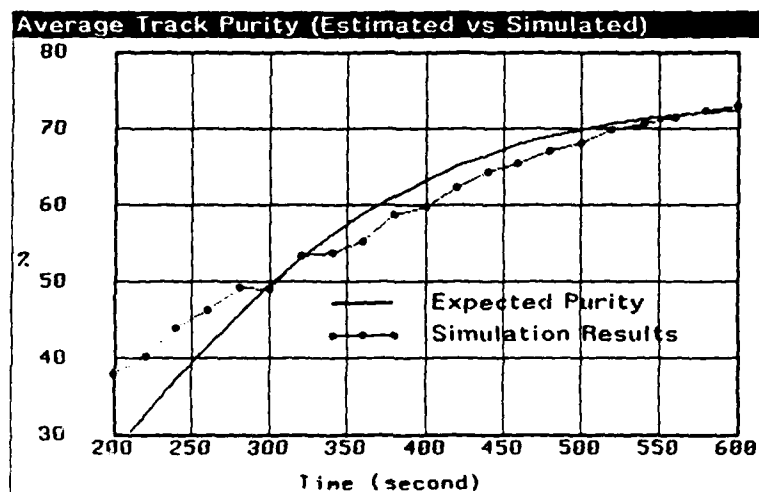this track. The track purity is calculated as the ratio of the number of measurements from the "true" origin over the total number of past detections contained in the track.

5. CONCLUSIONS

A very simple analytic model was developed for predicting the tracking performance in terms of average track purity, as a function of threat/sensor parameters. This model is based on a scaling law which describes the single-scan track-to-measurement correlation performance as a function of the object density on the sensor's focal plane and the average prediction error standard deviation. Fairly extensive Monte Carlo simulations were conducted to validate the analytic expression of the single-scan correlation performance. It was found that the Monte Carlo simulations support the predictions by our analysis very well in a reasonable range. Assuming a very simple tracking algorithm and relatively accurate *a priori* information, a limited number of small-scale tracking simulations were also conducted to verify the ability of our analytic models to predict track purity.

5.1 Achievements

The achievements of our research efforts can be summarized as follows:

1. Simple expressions were developed to assess single-scan track-to-measurement correlation performance and to estimate the performance of a given set of sensors against a given threat, in terms of average track purity.

2. Fairly extensive Monte-Carlo simulations support the simple analytic model for predicting single-scan track-to-measurement correlation performance.

3. The effects of eccentricity of the prediction error ellipses were examined to verify the calculation of correct association probability.

4. Uneven correlation performance due to A non-uniform object density was investigated.

5. The effects of false alarms were investigated. A simple extension to the analytic model was made to account for such effects. Fairly extensive Monte-Carlo simulations has shown the validity of this extension.

6. Cramér-Rao type lower bounds on state estimation error variance matrices as functions of a threat centroid trajectory and a sensor orbit were calculated to predict the track accuracy through tracking processes.

7. A simple model to describe object density on the sensor's focal plane was derived.

8. The average track purity as a function of time was calculated.

9. The effects of unresolved measurements were analyzed. In particular, a simple expression for the probability of measurement merging in terms of sensor resolutions and object densities was developed and incorporated into the calculation of the track purity.

10. Small-scale Monte-Carlo tracking simulations have demonstrated the validity of applying the simple analytic model to actual tracking system performance analysis.

5.2 Topics of Future Research

The issues deferred to future research are summarized as follows:

1. **Further development of analytic performance models**

   a. **Refine performance models:** As far as single-scan models are concerned, simple analytic models developed in the period covered by this report have been proved to be capable of accurately predicting correlation performance. There is, however, room for refinement in modeling multi-scan performance. In particular, the effects of mis-associations on the correlation performance in the subsequent scans should be investigated. The effects of unresolved measurements, mis-detections and false alarms need to be addressed in greater details.

   b. **Develop correlation stochastic models:** From the point of view from an object discrimination system, correlation statistics of track purity (both as a time series and as a sample set at one time) may be as important as the average track purity. Such correlation statistics may be obtained by analyzing interaction between correlation performance and prediction accuracy by tracks.

46

2. **Validation of analytic performance models:**

   a. **Validate by more extensive simulations:** Only a small number of test scenarios were conducted for the study described in this report. More studies extensive multi-scan (possibly multiple-sensor) simulations must be conducted. Through such studies key parameters in threat/sensor scenarios should be identified. Performance analysis should be extended to cover more difficult tracking situations with required accuracy, such as performance in autonomous track initiation phases.

   b. **Refine analytic model using simulation results:** Through such simulations, we may find needs for further refinement of analytic models or even for development of yet other models.

3. **System analysis:**

   a. **Develop models to parameterize sensor/threat geometry:** Since the number of parameters which completely describe a given threat/sensor scenario is not small and interaction among them is not simple, there is a need to identify key parameters which dominate the tracking performance.

   b. **Develop performance trade-off curves:** For system design purposes, performance trade-off curves may be found very useful. Analytic models developed in the current phase or the next phase of research may be used to produce several trade-off curves useful for sensor system design.

   c. **Investigate effects of track-initiation:** The impact of track initiation performance or of hand-over information should be further investigated. In particular, the effects of hand-over information or the lack of it are very important in designing the sensor systems for ballistic missile defense.

REFERENCES

[1] S. Mori, C.-Y. Chong, E. Tse, and R. P. Wishner, "Tracking and Classifying Multiple Targets without *A Priori* Identification," *IEEE Trans. on Automat. Contr.*, Vol. AC-31, No. 5, pp. 401 - 409, May 1986.

[2] C. B. Chang and L. C. Youens, "An Algorithm for Multiple Target Tracking and Data Correlation," Technical Report No. 643 (ESD-TR-83-017), Lincoln Laboratory, Massachusetts Institute of Technology, 1983. DTIC-AD-A131313/9.

[3] S. S. Blackman, *Multiple-Target Tracking with Radar Applications*, (Chap. 7. Analytic Techniques for System Evaluation), Artech House, Inc., 1986.

[4] Y. Bar-Shalom, et. al, "From Receiver Operating Characteristic to System Operating Characteristic: Evaluation of a Large Scale Surveillance System," CDC 87.

[5] Y. Bar-Shalom and T. Fortmann, *Tracking and Data Association*, Academic Press, 1988.

[6] P.W. Soule, "Performance of Two-Way Association of Complete Data Sets," Technical Report TOR-0074(4085)-15, The Aerospace Corporation, El Segundo, CA, Jan., 1974.

[7] J. Munkres, "Algorithm for the Assignment and Transportation Problems," *J. Soc. Indust. Appl. Math.*, Vol. 5, No. 1, pp. 32 - 38, March, 1957.

[8] K.-P. Dunn, "Lower Bounds on Acceleration Estimation Accuracy," Technical Report 790, M.I.T. Lincoln Laboratory, Lexington, MA, Oct., 1987.

[9] J. H. Taylor, "The Cramér-Rao Estimation Error Lower Bound Computation for Deterministic Nonlinear Systems," *IEEE Trans. on Auto. Contr.*, Vol. AC-24, No. 2, pp. 343 - 344, Apr., 1979.

[10] C. B. Chang and L. C. Youens, "An Algorithm for Multiple Target Tracking and Data Correlation," Technical Report 643, M. I. T. Lincoln Laboratory, Lexington, MA, June, 1983.

[11] C. B. Chang, K.-P. Dunn, and L. C. Youens, "A Tracking Algorithm for Dense Target Environments," *Proc. American Contr. Conf.*, pp. 613 - 618, June 1984.

[13] T. S. Lee, "Tracking in a Dense Environment: A Unified Treatment on Performance Analysis," *Proc. of 20-th Asilomar Conference on Signal, Systems & Computers*, pp. 403 - 408, Nov., 1986.

[14] K. Ito, *Probability Theory*, Chap. 4, Iwanami-Shoten, Tokyo, 1953.

[15] C. B. Chang and K. P. Dunn, "A Functional Model for the Closely Spaced Object Resolution Process," Technical Report 611, M. I. T. Lincoln Laboratory, Lexington, MA, May, 1982. DTIC-AD-A116890/5.

[16] C. B. Chang, "Ballistic Trajectory Estimation with Angle-Only Measurements," *IEEE Trans. on Auto. Contr.*, Vol. 25, No. 3, pp. 474 - 480, June 1980.

APPENDICES

A. Single-Scan Correlation Problem

This appendix shows how a correlation problem, in particular, a track-to-measurement correlation problem, can be formulated as a classical assignment problem. This fact has been treated as a trivial matter in the past in a majority of the multiple target tracking literature and seldom justified analytically. However, it might be worthwhile to examine the underlying assumptions which support this "fact."

As in Section 2.1, given a positive integer N, we assume three systems, $Y = (y_i)_{i=1}^N$, $\hat{Y} = (\hat{y}_i)_{i=1}^N$, and $Z = (z_i)_{i=1}^N$, of random vectors, and a random permutation π on the set $\{1, ..., N\}$, such that

$$P(Y, \hat{Y}, Z, \pi) = P(Y|Z, \pi)P(Z|\hat{Y})P(\pi)P(\hat{Y}) \tag{A.1}$$

with $P(\cdot)$ and $P(\cdot|\cdot)$ being the usual shorthand notation for the a probability (unconditional and conditional) distribution or its density. In other words, we assume a Markov chain, $\{\hat{Y} \rightarrow Z \rightarrow Y\}$, and that π is independent of $\hat{Y}$ and Z. The transition probabilities are given as

$$P\left((z_i)_{i=1}^N \in \prod_{i=1}^N dz_i \;\Big|\; (\hat{y}_i)_{i=1}^N\right) = \prod_{i=1}^N G(z_i - \hat{y}_i \;;\; Q_i)dz_i \tag{A.2}$$

and

$$P\left((y_i)_{i=1}^N \in \prod_{i=1}^N dy_i \;\Big|\; (z_i)_{i=1}^N, \pi\right) = \prod_{i=1}^N G(y_{\pi(i)} - z_i \;;\; R_{\pi(i)})dy_i \tag{A.3}$$

where $(Q_i)_{i=1}^N$ and $(R_j)_{j=1}^N$ are the two N-tuples of non-negative definite symmetric matrices, and $G(\cdot; V)$ is the probability density function for the zero-mean gaussian random vector with the variance matrix V.

The problem can then be described as a problem for determining an optimal estimate of the random permutation π given available data, $(Y, \hat{Y})$. The *maximum likelihood* (ML) *estimate*, $\hat{\pi}$, is an estimate which maximizes the likelihood,

$$
\begin{aligned}
P(Y, \hat{Y}|\pi) &= P(Y|\hat{Y}, \pi)P(\hat{Y}) \\
&= \int P(Y|Z, \pi)P(Z|\hat{Y})dZ\, P(\hat{Y}) \\
&= P((\hat{y}_i)_{i=1}^N) \prod_{i=1}^N G(y_{\pi(i)} - \hat{y}_i \;;\; S_{i\pi(i)})
\end{aligned} \tag{A.4}
$$

with $S_{ij} = Q_i + R_j$. Therefore, given $(Y, \hat{Y})$, a maximum likelihood estimate $\hat{\pi}$ should *minimize* the correlation cost function,

$$J(\pi) = \sum_{i=1}^N \|y_{\pi(i)} - \hat{y}_i\|^2_{S_{i\pi(i)}^{-1}} \tag{A.5}$$

assuming that all S_{ij}'s are positive definite. Moreover, if we assume that all the realizations of the random permutation π are equally likely, the maximum likelihood estimate is also a *maximum a posteriori probability* (MAP) *estimate*, since

$$P(\pi|Y, \hat{Y}) = \frac{P(Y, \hat{Y}|\pi)}{P(Y, \hat{Y})}P(\pi) = \frac{P(Y, \hat{Y}|\pi)}{P(Y, \hat{Y})}\frac{1}{N!} \tag{A.6}$$

We should note that this conclusion is totally independent of the *a priori* distribution, $P(\hat{Y})$. An alternative model can be constructed using

$$P(Y, \hat{Y}, Z, \pi) = P(Y|Z, \pi)P(\hat{Y}|Z)P(\pi)P(Z) \qquad (A.7)$$

instead of (A.1), and

$$P\left((\hat{y}_i)_{i=1}^N \in \prod_{i=1}^N d\hat{y}_i \;\Big|\; (z_i)_{i=1}^N\right) = \prod_{i=1}^N G(\hat{y}_i - z_i \; ; \; Q_i)d\hat{y}_i \qquad (A.8)$$

instead of (A.2). With this model, we have

$$P(Y, \hat{Y}|\pi) = \int P(Y|Z, \pi)P(\hat{Y}|Z)P(Z)dZ \qquad (A.9)$$

in place of (A.4). As we see in (A.9), if we can consider $P(Z)$ as constant, e.g., when $Z = (z_i)_{i=1}^N$ is i.i.d. with a common uniform distribution with a large enough support, the maximization of (A.9) is reduced to the minimization of the association function (A.5).

Thus either of these two different models actually support the association cost function (A.5). The difference between these two models can best described by the following two assumptions:

[$\mathcal{A}$1] $\hat{y}_1, ..., \hat{y}_N, n_1, ..., n_N, m_1, ..., m_N$, are independent from each other.

(which is stated in Section 2.1.), and

[$\mathcal{A}$2] $z_1, ..., z_N, n_1, ..., n_N, m_1, ..., m_N$, are independent from each other.

By a casual observation, the assumption [$\mathcal{A}$2] might look more "natural" than [$\mathcal{A}$1]. As seen in the next appendix, Appendix B, however, the first assumption will make further analysis much easier than the second one. However, we should remember that the model described in Section 2.1 and this appendix was to model a track-to-measurement association process in a multi-target tracking system. We will see in the following that with such a background the first assumption appears more appropriate.

Let us consider a more or less idealized situation in a multi-target tracking system. Suppose that we have been tracking N objects *perfectly*, i.e., that the N targets are independent, each object i has been uniquely associated with object-wise independent *information* I_i, and we have exactly N tracks so that the i-th track is the object state distribution conditioned by I_i. Let z_i be the "true" projection of the i-th object state onto the measurement space and let us assume that

$$P(z_i|I_i) = G(z_i - \hat{y}_i \; ; \; Q_i) \qquad (A.10)$$

which means[1]

$$\hat{y}_i = \mathcal{E}(z_i|I_i) \text{ and } Q_i = \mathcal{V}(z_i|I_i) \qquad (A.11)$$

Assuming the independent permutation π, the *a posteriori* probability of the permutation becomes

$$P(\pi \mid I, Y) = \frac{P(Y \mid \pi, I)}{P(Y \mid I)} P(\pi) \qquad (A.12)$$

---

[1] By $\mathcal{E}(\cdot|\cdot)$ and $\mathcal{V}(\cdot|\cdot)$, we mean the conditional mean and variance operators.

where $I = (I_i)_{i=1}^N$. Assuming that the random permutation π is totally random, in the sense of either the MAP or the ML, the track-to-measurement association problem becomes an optimization problem to maximize the likelihood function $P(Y|\pi, I)$. The assumption of independent measurement errors together with (A.11) leads to

$$P(Y \mid \pi, I) = \prod_{i=1}^{N} G\left(y_{\pi(i)} - \hat{y}_i \; ; \; S_{i\pi(i)}\right) \tag{A.13}$$

Apparently, the maximization of this quantity is equivalent to the minimization of the *correlation association cost function* (A.5).

Since $\hat{y}_i$ is the conditional expectation, it is orthogonal to the "prediction" error, $z_i - \hat{y}_i$, in the sense,

$$\mathcal{E}\left((z_i - \hat{y}_i)^T \hat{y}_i \mid I_i\right) = 0 \tag{A.14}$$

We may stretch this fact further to assume that the measurement prediction $\hat{y}_i$ is *independent* to the prediction error

$$m_i = z_i - \hat{y}_i \tag{A.15}$$

which should be zero-mean, gaussian with the variance matrix Q_i. This observation seems to support the assumption $[\mathcal{A}1]$ more than the other one $[\mathcal{A}2]$.

B. Calculation of Correct Association Probability

This appendix describes detailed derivations of the calculation of the correct association probability described in Section 2, and in particular, derivations of eqns. (2.7), (2.10) with (2.9) and the main result of Section 2, i.e., eqn. (2.13).

As in Section 2, we will first consider the cases where $N = 2$ and the random transposition (i.e., mis-association). Let us denote the event in which the two tracks are associated with correct measurements by E_{12}. Then this event can be identified with the following condition:

$$
\begin{aligned}
\Delta J &\overset{\text{def}}{=} J(\{(1,1),(2,2)\}) - J(\{(1,2),(2,1)\}) \\
&= \|y_1 - \hat{y}_1\|^2_{S_{11}^{-1}} + \|y_2 - \hat{y}_2\|^2_{S_{22}^{-1}} - \|y_1 - \hat{y}_2\|^2_{S_{21}^{-1}} - \|y_2 - \hat{y}_1\|^2_{S_{12}^{-1}} \\
&= \|n_1 - m_1\|^2_{(S_{11}^{-1} - S_{21}^{-1})} + \|n_2 - m_2\|^2_{(S_{22}^{-1} - S_{12}^{-1})} - \|\hat{y}_1 - \hat{y}_2\|^2_{(S_{12}^{-1} + S_{21}^{-1})} \\
&\quad + 2(S_{12}^{-1}(n_2 - m_2) - S_{21}^{-1}(n_1 - m_1))^T(\hat{y}_1 - \hat{y}_2) \\
&\leq 0
\end{aligned}
\tag{B.1}
$$

We may calculate the (conditional) characteristic function, $\psi(\zeta) \overset{\text{def}}{=} \mathcal{E}(e^{\jmath \Delta J \zeta}|\hat{y}_1, \hat{y}_2)$, of the random variable ΔJ as

$$
\begin{aligned}
\psi(\zeta) &= (\det(2\pi S_{11})\det(2\pi S_{22}))^{-1/2} \cdot \exp\left(-\jmath\|\hat{y}_1 - \hat{y}_2\|^2_{S_{12}^{-1} + S_{21}^{-1}}\right) \cdot \\
&\quad \int_{\mathcal{R}^4} \exp\left(\jmath\left(\|u_1\|^2_{(S_{11}^{-1} - S_{21}^{-1})} + \|u_2\|^2_{(S_{22}^{-1} - S_{12}^{-1})} + 2(S_{12}^{-1}u_2 + S_{21}^{-1}u_1)^T(\hat{y}_1 - \hat{y}_2)\right)\right) \\
&\quad \cdot \exp\left(-\frac{1}{2}\left(\|u_1\|^2_{S_{11}^{-1}} + \|u_2\|^2_{S_{22}^{-1}}\right)\right) du_1 du_2
\end{aligned}
\tag{B.2}
$$

which can be expressed in a closed form. Then, using some form of numerical integration, possibly by an FFT program, we can calculate

$$
\text{Prob.}\{E_{12}|\hat{y}_1, \hat{y}_2\} = \text{Prob.}\{\Delta J \leq 0|\hat{y}_1, \hat{y}_2\} = \frac{1}{2\pi}\int_{-\infty}^{0}\int_{-\infty}^{\infty} e^{-\jmath z \zeta}\psi(\zeta)d\zeta \, dz
\tag{B.3}
$$

The results of such a calculation is described in [6]. Although one can make several interesting observations from results of such numerical analysis, it is not easy to extend the results beyond the simplified two-object cases or to relate the results to key parameters in track-to-measurement association problems.

On the other hand, if we assume

$$
S \overset{\text{def}}{=} S_{11} = S_{22} = S_{12} = S_{21}
\tag{B.4}
$$

(B.1) becomes

$$
\begin{aligned}
\Delta J &= -2(y_1 - y_2)^T S^{-1}(\hat{y}_1 - \hat{y}_2) \\
&= 2(m_1 - m_2 - (n_1 - n_2) - (\hat{y}_1 - \hat{y}_2))^T S^{-1}(\hat{y}_1 - \hat{y}_2) \\
&= 2(w - \|\hat{y}_1 - \hat{y}_2\|^2_{S^{-1}}) \\
&\leq 0
\end{aligned}
\tag{B.5}
$$

54

where $w = (m_1 - m_2 - n_1 + n_2)^T S^{-1}(\hat{y}_1 - \hat{y}_2)$. Since we have assumed that m_i's and n_i's are independent of $\hat{y}_i$'s, w is gaussian given $\hat{y}_1$ and $\hat{y}_2$ with

$$\mathcal{E}(w|\hat{y}_1, \hat{y}_2) = 0 \tag{B.6}$$

and

$$\mathcal{V}(w|\hat{y}_1, \hat{y}_2) = 2\|\hat{y}_1 - \hat{y}_2\|_{S^{-1}}^2 \tag{B.7}$$

from which eqn. (2.7) follows.

In order to calculate the unconditional probability, Prob.(E_{12}), we need a mathematical model for $(\hat{y}_1, \hat{y}_2)$. For this, let us assume that the two random vectors are independent and have a common distribution which is uniform on a disk with the center at the origin and with a given radius r. Before considering Prob.(E_{12}), let us consider a more restricted problem of finding a conditional probability Prob.$(E_{12}|\hat{y}_1 = 0)$. Since $\hat{y}_2$ is independent of $\hat{y}_1$, (even with the condition $\hat{y}_1 = 0$) $\hat{y}_2$ is uniformly distributed on the disk. Thus it follows from (2.7) that

$$
\begin{aligned}
\text{Prob}(E_{12} \mid \hat{y}_1 = 0) &= (\pi r^2)^{-1} \int_{\{\|\hat{y}_2\| \leq r\}} \text{erf}\left(\frac{\|\hat{y}_2\|_{S^{-1}}}{\sqrt{2}}\right) d\hat{y}_2 \\
&= 1 - (\pi r^2)^{-1} \int_{\{\|\hat{y}_2\| \leq r\}} \text{erfc}\left(\frac{\|\hat{y}_2\|_{S^{-1}}}{\sqrt{2}}\right) d\hat{y}_2
\end{aligned}
\tag{B.8}
$$

where $\text{erfc}(\xi) = 1 - \text{erf}(\xi)$. Without loss of generality, we can assume $S = \text{Diag.}[a^2, b^2]$, with $a \geq b$. If S is not diagonal, we can always diagonalize it by properly rotating the coordinate without changing the integral. Thus, with a coordinate transformation, $\hat{y}_2 = [\rho \cos\theta, \rho \sin\theta]^T$, we have

$$
\begin{aligned}
\int_{\{\|\hat{y}_2\| \leq r\}} \text{erfc}\left(\frac{\|\hat{y}_2\|_{S^{-1}}}{\sqrt{2}}\right) d\hat{y}_2 &= \int_0^r \int_0^{2\pi} \text{erfc}(U(\theta)\rho) d\theta \rho d\rho \\
&= \int_0^{2\pi} \left[\int_0^r \text{erfc}(U(\theta)\rho)\rho d\rho\right] d\theta \\
&= \int_0^{2\pi} U(\theta)^{-2} \, I(U(\theta)r) \, d\theta
\end{aligned}
\tag{B.9}
$$

where

$$U(\theta) \overset{\text{def}}{=} \frac{1}{\sqrt{2}} \frac{\|\hat{y}_2\|_{S^{-1}}}{\|\hat{y}_2\|} = \sqrt{\frac{1}{2}\left(\frac{\cos^2\theta}{a^2} + \frac{\sin^2\theta}{b^2}\right)} \tag{B.10}$$

and

$$
\begin{aligned}
I(x) &\overset{\text{def}}{=} \int_0^x \text{erfc}(\xi)\xi d\xi \\
&= \frac{1}{4} + \frac{1}{2}\left[(x^2 - 1)\text{erfc}(x) - \frac{1}{\sqrt{2\pi}} x \exp\left(-\frac{1}{2}x^2\right)\right] \\
&= \frac{1}{4} + O\left(x^{-1} e^{-x^2/2}\right)
\end{aligned}
\tag{B.11}
$$

Figure B-1 show the function $I(\cdot)$ defined by (B.11). As we see in this figure, this
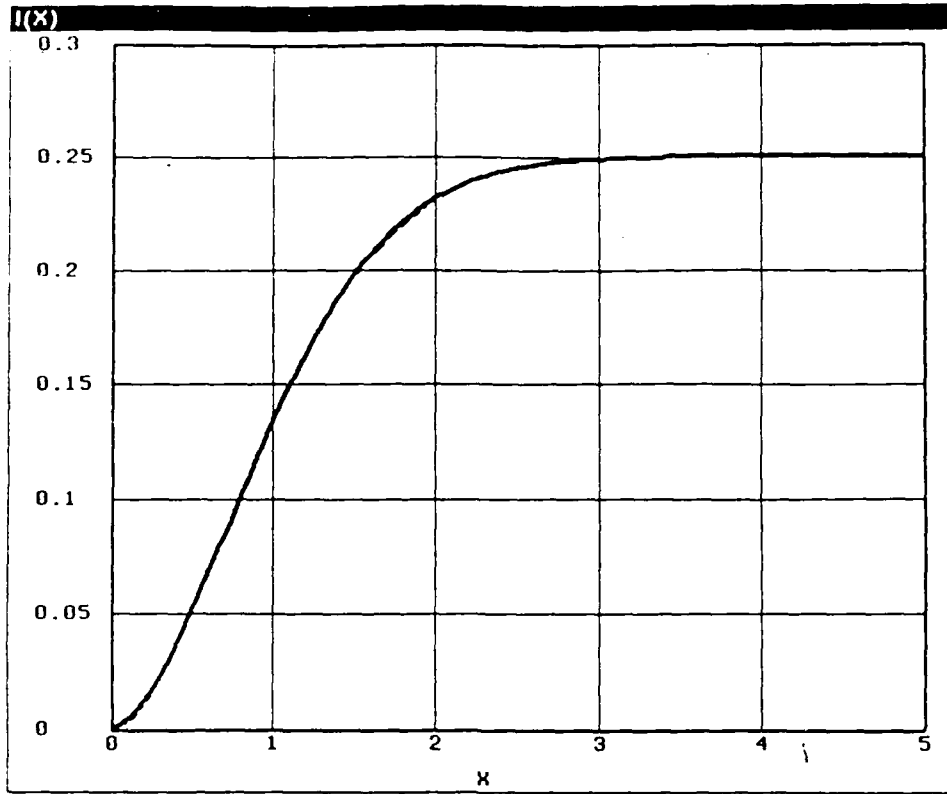
Figure B-1: Integral $I(x)$

function converges to its asymptotic value, 1/4, approximately at 3 (corresponding to the 3-σ point). On the other hand, we have

$$\int_0^{2\pi} U(\theta)^{-2} d\theta = 8 \int_0^{\pi/2} \frac{d\theta}{a^{-2} \cos^2(\theta) + b^{-2} \sin^2(\theta)} = 4\pi ab \qquad \text{(B.12)}$$

Since $\sqrt{2} U(\theta) \geq 1/a$ for all θ, it follows from eqns. (B.8) through (B.12) that

$$\text{Prob.}(E_{12} \mid \hat{y}_1 = 0) = 1 - \frac{ab}{r^2} + O\left(r^{-3} e^{-(1/4)(r/a)^2}\right) \qquad \text{(B.13)}$$

Now let us consider the unconditional probability: It follows from (2.7) and the i.i.d.-uniform assumption that

$$\begin{aligned}
\text{Prob.}(E_{12}) &= (\pi r^2)^{-2} \int_{\{\|\hat{y}_1\| \leq r\}} \int_{\{\|\hat{y}_2\| \leq r\}} \text{erf}\left(\frac{\|\hat{y}_1 - \hat{y}_2\|_{S^{-1}}}{\sqrt{2}}\right) d\hat{y}_1 d\hat{y}_2 \\
&= (\pi r^2)^{-1} \int_{\{\|\hat{y}_1\| \leq r\}} W(\hat{y}_1) d\hat{y}_1
\end{aligned} \qquad \text{(B.14)}$$

where

$$W(\hat{y}_1) \overset{\text{def}}{=} (\pi r^2)^{-1} \int_{\{\|\eta - \hat{y}_1\| \leq r\}} \text{erf}\left(\frac{\|\eta\|_{S^{-1}}}{\sqrt{2}}\right) d\eta \qquad \text{(B.15)}$$

Using the same argument as the one which has lead us to (B.13), we may conclude the function $W(\hat{y}_1)$ can be well approximated by a constant function, i.e., $W(0)$ which is nothing

56

but (B.13), if $\|\hat{y}_1\| \ll r$ or practically $\|\hat{y}_1\| \leq r - 3a$. In other words, *except for the cases where $\hat{y}_1$ locates on the peripheral of the disk*, we can approximate $W(\hat{y}_1) = \text{Prob.}(E_{12}|\hat{y}_1)$ by $W(0)$. Since the area of the periphery is proportional to r while the whole area of the disk is proportional to r^2, when averaging over $\hat{y}_1$, we can ignore this *edge effect*. Noting $\det(S) = a^2 b^2$, we have proved that, for large enough r, we have (2.10) with (2.9).

Now suppose that the number N of objects is a random integer having a Poisson distribution with mean ν and assume that the approximation

$$\text{Prob.}(E_c \mid N = n) \approx \left(1 - \left(\frac{\bar{\sigma}}{r}\right)^2\right)^{n-1} \tag{B.16}$$

is valid where E_c is the event where a track is associated with the correct measurement (following the *reasoning* described in Section 2.1). Then, defining E_c such that $\text{Prob.}(E_c|N = 0) = \text{Prob.}(E_c|N = 1) = 1$, we have

$$
\begin{aligned}
\text{Prob.}(E_c) &\approx e^{-\nu}\left[1 + \sum_{n=1}^{\infty} \frac{\nu^n \left(1 - \left(\frac{\bar{\sigma}}{r}\right)^2\right)^{n-1}}{n!}\right] \\
&= \frac{e^{-\nu\left(\frac{\bar{\sigma}}{r}\right)^2} - \left(\frac{\bar{\sigma}}{r}\right)^2 e^{-\nu}}{1 - \left(\frac{\bar{\sigma}}{r}\right)^2} \\
&\approx \exp\left(-\nu\left(\frac{\bar{\sigma}}{r}\right)^2\right) = \exp(-\pi\beta\bar{\sigma}^2)
\end{aligned} \tag{B.17}
$$

which is actually eqn. (2.13). The last step of the above derivation uses the approximation based on the assumption $\bar{\sigma} \ll r$. The β is the object density defined by (2.14).

C. Effects of Non-Uniform Local Object Density

In Appendix B, we derived a simple scaling law to determine the probability of correct association as a function of object density and track measurement prediction errors. To do so, we have assumed objects are distributed uniformly on a given region of the sensor's focal plane. This uniformity assumption may not validly reflect reality. For example, if objects are distributed uniformly within a ball in a three-dimensional space, apparently their projections onto a (2-dim.) plane will not have uniform density.

In this appendix, we will calculate the probability of correct association for a group of targets distributed spatially with a gaussian distribution instead of uniform distribution. As we did in Appendix B, we will first consider the transposition in the two-object model. We assume that the two-dimensional gaussian vectors, $\hat{y}_1$ and $\hat{y}_2$, are independent but share a common zero mean gaussian distribution with a variance matrix V. In order to examine the effect of this "uneven" (or non-uniform) spatial distribution, we would like to calculate the probability of a given track, say the first track, being correctly associated with a measurement when conditioned by the position of the track, i.e., Prob.$(E_{12}|\hat{y}_1)$. For the sake of simplicity, we assume that the spatial variation matrix V is diagonal as $V = \Sigma^2 I$ and that the average prediction error variance matrix S is (at least approximately) diagonal as $S = \bar{\sigma}^2 I$. With these simplifying assumptions, the conditional probability, Prob.$(E_{12}|\hat{y}_1)$, is only a function of $\|\hat{y}_1\|$. Thus the purpose of this appendix is to calculate the conditional probability, Prob.$(E_{12}|\|\hat{y}_1\| = r)$.

It follows from (2.7) and the above assumptions that

$$\text{Prob.}(E_{12} \mid \|\hat{y}_1\| = r) = \mathcal{E}\left(\text{erf}\left(\frac{\|\hat{y}_1 - \hat{y}_2\|}{\sqrt{2}\bar{\sigma}}\right) \;\middle|\; \|\hat{y}_1\| = r\right) = \int_0^\infty \text{erf}\left(\frac{\rho}{\sqrt{2}\bar{\sigma}}\right) f(\rho)d\rho \quad \text{(C.1)}$$

where f is the probability density function of $\|\hat{y}_1 - \hat{y}_2\|$ given the condition $\|\hat{y}_1\| = r$, i.e.,

$$f(\rho) = \frac{\rho}{\Sigma^2}\exp\left(\frac{-(\rho^2 + r^2)}{2\Sigma^2}\right) I_0\left(\frac{\rho r}{\Sigma^2}\right) \quad \text{(C.2)}$$

with $I_0(\cdot)$ being the modified Bessel's function defined by

$$I_0(x) = \sum_{n=0}^\infty \frac{x^{2n}}{2^{2n}(n!)^2} \quad \text{(C.3)}$$

It follows from (C.1) that

$$
\begin{aligned}
P(E_{12} \mid \|\hat{y}_1\| = r) &= \int_0^\infty \text{erf}\left(\frac{\rho}{\sqrt{2}\bar{\sigma}}\right) \frac{\rho}{\Sigma^2}\exp\left(\frac{-(\rho^2 + r^2)}{2\Sigma^2}\right) I_0\left(\frac{\rho r}{\Sigma^2}\right) d\rho \\
&= \exp\left(\frac{-r^2}{2\Sigma^2}\right) \int_0^\infty \frac{2\bar{\sigma}^2}{\Sigma^2}\text{erf}(x)x\exp\left(\frac{\bar{\sigma}^2}{\Sigma^2}x^2\right) I_0\left(\frac{\sqrt{2}\bar{\sigma}r}{\Sigma^2}x\right) dx \\
&= \exp\left(\frac{-r^2}{2\Sigma^2}\right) \alpha\sum_{n=0}^\infty C_n \int_0^\infty \text{erf}(x)x^{2n+1}\exp\left(-\frac{1}{2}\alpha x^2\right) dx \\
&= \exp\left(\frac{-r^2}{2\Sigma^2}\right) \sum_{n=0}^\infty K_n
\end{aligned}
\quad \text{(C.4)}
$$

58

where $\alpha = \dfrac{2\bar{\sigma}^2}{\Sigma^2}$, $C_n = \dfrac{\gamma^{2n}}{2^{2n}(n!)^2}$, $\gamma = \dfrac{\sqrt{2}\bar{\sigma}r}{\Sigma^2}$, and

$$K_n \stackrel{\text{def}}{=} \alpha C_n \int_0^\infty \text{erf}(x) x^{2n+1} \exp\left(-\frac{1}{2}\alpha x^2\right) dx \tag{C.5}$$

The sequence $\{K_n\}$ can be calculated recursively as shown below: First we should note

$$\int_0^\infty \exp(-ax^2) x^{2n} dx = \frac{(2n-1)!!}{2^{n+1}}\sqrt{\frac{\pi}{a^{2n+1}}} \tag{C.6}$$

Integrating (C.5) by parts and using the above equality, we have

$$K_n = \frac{\gamma^2}{2n\alpha}K_{n-1} + \frac{\gamma^{2n}}{(\alpha+1)^{n+1/2}}\frac{(2n-1)!!}{2^{2n+1}(n!)^2} \tag{C.7}$$

where $(2n-1)!! \stackrel{\text{def}}{=} (2n-1)\cdot(2n-3)\cdots 3\cdot 1$, and

$$K_0 = \frac{1}{2}\left[1 + \frac{\Sigma}{\sqrt{\Sigma^2 + 2\bar{\sigma}^2}}\right] \tag{C.8}$$

We can calculate the conditional probability (C.4), first by calculating the sequence $\{K_n\}$ by (C.7) and then by putting the results into (C.4). However, an approximate but more concise expression is desirable. In order to obtain such an approximate expression, we will look for appropriate upper and lower bounds on the series $\sum_{n=0}^\infty K_n$. First let us rewrite (C.7) as

$$K_n = \frac{\gamma^2}{2n\alpha}K_{n-1} + \frac{\gamma^{2n}}{2^{n+1}(\alpha+1)^{n+1/2}}\frac{\Gamma(n+\frac{1}{2})}{[\Gamma(n+1)]^2} \tag{C.9}$$

Then define two sequences, $\{K'_n\}$ and $\{K''_n\}$, by

$$K' = \frac{p}{n}K'_{n-1} + \frac{q^n}{n!} \tag{C.10}$$

and

$$K'' = \frac{p}{n}K''_{n-1} \tag{C.11}$$

where $p = \dfrac{\gamma^2}{2\alpha}$, $q = \dfrac{\gamma^2}{2(1+\alpha)}$, and $K'_0 = K''_0 = K_0$. Obviously, we have,

$$\sum_{n=0}^\infty K''_n \leq \sum_{n=0}^\infty K_n \leq \sum_{n=0}^\infty K'_n \tag{C.12}$$

On the other hand, we have $\sum_{n=0}^\infty K''_n = K_0 e^p$, and

$$
\begin{aligned}
\sum_{n=0}^\infty K'_n &= K_0 e^p + \frac{q}{p}(e^p - 1) + \frac{q^2}{p^2}(e^p - 1 - p) + \ldots \\
&\leq K_0 e^p + (e^p - 1)\left(\frac{q}{p} + \frac{q^2}{p^2} + \frac{q^3}{p^3} + ..\right) \\
&= K_0 e^p + \alpha(e^p - 1)
\end{aligned}
\tag{C.13}
$$

Therefore, from (C.12) and (C.13), we have,

$$K_0(e^p - 1) \le \sum_{n=1}^{\infty} K_n \le (K_0 + \alpha)(e^p - 1) \tag{C.14}$$

Then, assuming $\bar{\sigma} \ll \Sigma$, or equivalently $\alpha \ll 1$, we can make the approximations, $\alpha \approx 0$, $K_0 \approx 1$, and hence

$$\sum_{n=1}^{\infty} K_n \approx e^p - 1 \tag{C.15}$$

It follows from (C.4) and from this approximation that

$$P(E_{12} \mid \|\hat{y}_1\| = r) \approx \exp\left(\frac{-r^2}{2\Sigma^2}\right)\left(K_0 + \exp\left(\frac{r^2}{2\Sigma^2}\right) - 1\right) \approx 1 - \frac{1}{2}\left(\frac{\bar{\sigma}}{\Sigma}\right)^2 \exp\left(\frac{-r^2}{2\Sigma^2}\right) \tag{C.16}$$

When the total number, N, of targets is random and has a Poisson distribution with mean ν, the overall correct association probability can be calculated as

$$
\begin{aligned}
\text{Prob.}(E_c \mid \|\hat{y}_1\| = r) &= \sum_{n=1}^{\infty} \text{Prob.}(E_c \mid \|\hat{y}_1\| = r, N = n)\text{Prob.}\{N = n\} \\
&= \exp\left(-\nu(1 - \text{Prob.}(E_{12} \mid \|\hat{y}_1\| = r))\right) \\
&= \exp\left(-\frac{\nu}{2}\left(\frac{\bar{\sigma}}{\Sigma}\right)^2 \exp\left(\frac{-r^2}{2\Sigma^2}\right)\right) \\
&= \exp(-\pi\beta(r)\bar{\sigma}^2)
\end{aligned}
\tag{C.17}
$$

where $\beta(r)$ is the object density at points with distance r from the object group's center and expressed as

$$\beta(r) = \frac{\nu}{2\pi\Sigma^2}\exp\left(\frac{-r^2}{2\Sigma^2}\right) \tag{C.18}$$

60

D. Effects of False Alarms

In this appendix, we will calculate the probability of correct association in the presence of false alarms. As we did in Section 2.2 and Appendix B, let us consider an object, say the first object, situated at origin, in the sense that $\hat{y}_1 = 0$. Then, suppose that there are $N - 1$ other objects and N_f false alarms, both N and N_f being random. We assume that the two random integers, N and N_f, are independent and have Poisson distributions with mean, ν and ν_f, respectively. Given N and N_f, the joint system, $\{\{\hat{y}_i\}_{i=2}^{N}, \{y_i^{FA}\}_{i=1}^{N_f}\}$ of other objects, $\{\hat{y}_i\}_{i=1}^{N}$, and false alarms, $\{y_i^{FA}\}_{i=1}^{N_f}$, is assumed to be independent and has an identical uniform distribution on the disk centered at the origin with radius r.

As before, let E_c be the event in which the first object is associated with the correct measurement. Then, since the objects and false alarms are independent from each other, we have

$$\text{Prob.}(E_c) = \text{Prob.}(E_{ct})\text{Prob.}(E_{cf}) \tag{D.1}$$

where E_{ct} is the event in which there is no transposition among objects involving the first one, and E_{cf} is the event in which there is no switch between the true measurement from the first object and any of the false alarms. Since both events are independent from each other, the results of Appendix B implies

$$\text{Prob.}(E_{ct}) \approx \exp(-\pi\beta\bar{\sigma}^2) \tag{D.2}$$

where $\beta = \dfrac{\nu}{\pi r^2} \approx \dfrac{\nu - 1}{\pi r^2}$ is the object density. The rest of this appendix describes the second factor, $\text{Prob.}(E_{cf})$, in (D.1).

Let P_{f1} be the probability that, given a false alarm and the correct measurement, the false alarm is not associated with the first track, i.e., the likelihood of associating the true measurement is higher than the likelihood of associating the false alarm. Then, under the condition where there are n false alarms and just one track, the probability that the track is associated with the correct measurement (i.e., with none of the false alarms) is $(P_{f1})^n$. Therefore, when we take expectation over the distribution of the number of false alarms, we have

$$\text{Prob.}(E_{cf}) = e^{-\nu_f} \sum_{n=0}^{\infty} \frac{(\nu_f)^n}{n!} (P_{f1})^n = \exp\left(-\nu_f(1 - P_{f1})\right) \tag{D.3}$$

We can write the probability P_{f1} explicitly as

$$P_{f1} = \text{Prob.}\{\|y_1 - \hat{y}_1\|_{S^{-1}}^2 \leq \|y_f - \hat{y}_1\|_{S^{-1}}^2\} \tag{D.4}$$

where y_1 is the true measurement which should be associated with the track which has the prediction at $\hat{y}_1$, y_f is a false alarm, and S is the average prediction error variance matrix satisfying (B.4). Moreover, for the sake of simplicity, we assume that the average prediction error variance matrix S is diagonal as $S = \bar{\sigma}^2 I$ at least approximately, with $\bar{\sigma}$ being the average prediction error standard deviation. With the assumption $\hat{y}_1 = 0$, we have

$$P_{f1} = \text{Prob.}\{\|y_1\|^2 \leq \|y_f\|^2\} = \text{Prob.}\{\|y_1\| \leq \|y_f\|\} \tag{D.5}$$

61

Let $\rho_1 = \|y_1\|$ and $\rho_f = \|y_f\|$. It can be easily shown that the probability density functions of ρ_1 and ρ_f are

$$p_1(\rho_1) = \frac{\rho_1}{\bar{\sigma}^2}\exp\left(-\frac{\rho_1^2}{2\bar{\sigma}^2}\right) \tag{D.6}$$

and

$$p_f(\rho_f) = \frac{2\rho_f}{r^2} \tag{D.7}$$

respectively, with the same support, $[0, r]$. Therefore, it follows from (D.5) that

$$
\begin{aligned}
P_{f1} &= \int_{\{(\rho_1,\rho_f)\in[0,r]^2\,|\,\rho_1\leq\rho_f\}} p_1(\rho_1)p_f(\rho_f)\,d\rho_1 d\rho_f \\
&= \int_0^r \left(\int_0^{r_f} p_1(r_1)dr_1\right) p_f(r_f)dr_f \\
&= 1 - \frac{2\bar{\sigma}^2}{r^2}\left(1 - \exp\left(-\frac{r^2}{2\bar{\sigma}^2}\right)\right) \\
&\approx 1 - \frac{2\bar{\sigma}^2}{r^2}
\end{aligned}
\tag{D.8}
$$

In the last step, an approximation based on $R \gg \sigma$ has been used.

Now, it follows from (D.3) and (D.8) that

$$\text{Prob.}(E_{cf}) = \exp\left(-\nu_f\frac{2\bar{\sigma}^2}{r^2}\right) = \exp\left(-2\pi\beta_{FA}\bar{\sigma}^2\right) \tag{D.9}$$

where $\beta_{FA} = \frac{\nu_f}{\pi r^2}$ is the false alarm density. Therefore, from (D.1), (D.2), and (D.9), the overall correct association probability becomes,

$$\text{Prob.}(E_c) = \exp\left(-\pi(\beta + 2\beta_{FA})\bar{\sigma}^2\right) \tag{D.10}$$

E. Orbital Dynamics and Observation

This appendix describes the dynamics and the observation functions, f and h in Section 3, for different coordinate systems shown in Table 3-1.

In the cartesian coordinate system, eqn. (3.1) is Newton's equation for the two-body problem with $x(t)$ being the 3D position and velocity at time t. Thus we have

$$f(x) = f\left(\begin{bmatrix} u \\ v \end{bmatrix}\right) = \begin{bmatrix} v \\ -\gamma \dfrac{u}{\|u\|^3} \end{bmatrix} \tag{E.1}$$

where γ is the earth gravity constant. The observation function $h(\cdot, t)$ at time t maps the vector $x(t) - x_s(t)$ into the angular projection, i.e., the azimuth-elevation pair, where $x_s(t)$ is the 3D position of the sensor at the time. The partial derivatives are then calculated as

$$\frac{\partial f}{\partial x}(x) = \frac{\partial f}{\partial x}\left(\begin{bmatrix} u \\ v \end{bmatrix}\right) = \begin{bmatrix} 0 & I \\ -\dfrac{\gamma}{\|u\|^3}\left(I - 3\dfrac{uu^T}{\|u\|^2}\right) & 0 \end{bmatrix} \tag{E.2}$$

and[1]

$$\frac{\partial h}{\partial x}(x, t) = \|x(t) - x_s(t)\|^{-1} \begin{bmatrix} e^T & 0 \\ g^T & 0 \end{bmatrix} \tag{E.3}$$

where $\{e, g\}$ is the system of ortho-normal vectors which are orthogonal to $x(t) - x_s(t)$.

When we choose a coordinate system such that $x(t)$ is the range $R(t)$, the azimuth $A(t)$ and the elevation $E(t)$, and their rates, $\dot{R}(t)$, $\dot{A}(t)$ and $\dot{E}(t)$, the dynamics represented by f becomes very complicated. According to [16], we have

$$\ddot{R} = R(\dot{E}^2 + \dot{A}^2 \cos^2 E) - \frac{\gamma \sin E}{R_s^2}\left[\frac{R_s^2(R + R_e \sin E)}{R_T^3 \sin E} - 1\right]$$

$$\ddot{A} = -2\frac{\dot{R}}{R}\dot{A} + 2\dot{A}\dot{E}\tan E \tag{E.4}$$

$$\ddot{E} = -2\frac{\dot{R}}{R}\dot{E} - \frac{\dot{A}^2}{2}\sin 2E - \frac{\gamma \cos E}{RR_s^2}\left[\left(\frac{R_s}{R_T}\right)^3 - 1\right]$$

where $R_T = (R^2 + R_s^2 + 2RR_s \sin E)^{1/2}$ is the distance of the object from the earth's center, R_s is the distance between the sensor and the earth's center, and R_e is the radius of the earth. The partial derivatives of f is thus very complicated. On the other hand, the observation function h becomes a simple projection with partials

$$\frac{\partial h}{\partial x}(x, t) = \begin{bmatrix} 0 & 1 & 0 & 0 & 0 & 0 \\ 0 & 0 & 1 & 0 & 0 & 0 \end{bmatrix} \tag{E.5}$$

When the six orbital elements are used for the object state variable $x(t)$, the dynamics become very simple. For example, if we use the mean anomaly, the mean anomaly rate, the

---

[1] I is the identity matrix with appropriate dimension, in this case three.

angular momentum (or the eccentricity), and three parameters to determine the orbital plane and the perigee direction, all the variables except one (the mean anomaly) are constant, and the dynamics are simply expressed as that the time derivative of the mean anomaly is the constant mean anomaly rate. Thus the partials of f are

$$
\frac{\partial f}{\partial x}(x) = \begin{bmatrix} 0 & 1 & 0 & 0 & 0 & 0 \\ 0 & 0 & 0 & 0 & 0 & 0 \\ 0 & 0 & 0 & 0 & 0 & 0 \\ 0 & 0 & 0 & 0 & 0 & 0 \\ 0 & 0 & 0 & 0 & 0 & 0 \\ 0 & 0 & 0 & 0 & 0 & 0 \end{bmatrix} \tag{E.6}
$$

The observation function h becomes the composition of the transformation from the orbital elements to the cartesian and then from cartesian to the angular measurement. The partial derivatives can be obtained by post-multiplying the partials of the orbital-element-to-cartesian transformation from the right of (E.3).

F. Calculation of Probability of Measurement Merging

This appendix describes the derivation of (4.8), i.e., the probability of an object being unresolved with another object on a given focal plane of a sensor, in Section 4.2. For the derivation, we will use the following mathematical model:

1. There are N objects on the focal plane where N is a random integer having a Poisson distribution with mean ν.

2. Given the number N of objects, the objects are model by an i.i.d. system, $\{z_i\}_{i=1}^{N}$, with a common distribution which is uniform on the disk centered at the origin and with radius r.

3. The probability of merging two objects, at y_1 and y_2, are given by $p_m(\|y_1 - y_2\|)$, where p_m is a continuously decreasing function such that $p_m(0) = 1$ and $p_m(\rho) = 0$ for $\rho > \delta$ with δ being the sensor resolution. In particular, we will adopt a piecewise linear model described by (4.6) in Section 4.2. (See Figure 4-1.)

4. We assume that $\nu \gg 1$ and $r \gg \delta$ but the object density

$$\beta = \frac{\nu}{\pi r^2}$$

is comparable to 1 with respect to the resolution cell area, δ^2, i.e.,

$$\beta \delta^2 = \frac{\nu}{\pi} \left(\frac{\delta}{r}\right)^2$$

is comparable to 1.

Let E_M be the event in which an object, say the first object, z_1, is merged with (unresolved from) at least one of other objects, $z_2, ..., z_N$, i.e.,

$$E_M = \cup_{i=2}^{N} E_M^{(1,i)} \tag{F.1}$$

where $E_M^{(1,i)}$ is the event in which the first object is merged with the i-th object. Unfortunately, it is not easy to calculate the probability, P_M, of the event E_M mainly because the $E_M^{(1,i)}$'s are not disjoint. In order to overcome this difficulty, we will approximate the event E_M by $E_M^{(1,\tilde{\imath})}$ where $\tilde{\imath}$ is the index of the nearest neighbor object $z_{\tilde{\imath}}$ from z_1. The validity of this approximation is tested by Monte Carlo runs, the results of which are shown in Section 4.2. (See Figure 4-2.) With this approximation, we may calculate the probability, P_M, of measurement merging as

$$
\begin{aligned}
P_M &\stackrel{\text{def}}{=} \text{Prob.}(E_M) \\
&\approx \text{Prob.}(E_M^{(1,\tilde{\imath})}) \\
&= \text{Prob.}(E_M^{(1,\tilde{\imath})} \mid N \geq 2)\text{Prob.}\{N \geq 2\} \\
&\approx \int_0^r p_m(\rho)q(\rho)d\rho \\
&= \int_0^\delta p_m(\rho)q(\rho)d\rho
\end{aligned}
\tag{F.2}
$$

where q is the probability density function for the distance to the nearest neighbor defined by

$$q(\rho)d\rho \overset{\text{def}}{=} \text{Prob.}\{\|z_i\| \in d\rho \mid N \geq 2\} \tag{F.3}$$

In the last step of (F.2), we used the fact $\nu \gg 1$.

Thus we will first calculate the distribution of the distance from the first object z_1 to its nearest neighbor z_i. Assuming a large enough radius r of the extent of the objects, we can let $z_1 = 0$. Other objects, $z_2, ..., z_N$, form an i.i.d. system with the uniform distribution on a disk, and hence,

$$p(\rho)d\rho \overset{\text{def}}{=} \text{Prob.}\{\|z_i\| \in d\rho\} = 2\frac{\rho}{r^2}d\rho \tag{F.4}$$

for $\rho \in [0, r]$. Therefore, the distribution of the distance to the nearest neighbor object (from the first object) can be expressed as

$$p_n(\rho)d\rho \overset{\text{def}}{=} \text{Prob.}\{\|z_i\| \in d\rho \mid N = n+1\} = \frac{2n\rho(r^2 - \rho^2)^{n-1}}{r^{2n}}d\rho \tag{F.5}$$

for $\rho \in [0.r]$ and for $n \geq 1$. Since we are assuming that the number N of object has the Poisson distribution with mean ν, we have

$$
\begin{aligned}
q(\rho) &= \frac{\displaystyle\sum_{n=1}^{\infty} \frac{\nu^{(n+1)}}{(n+1)!} \frac{2n\rho(r^2 - \rho^2)^{n-1}}{r^{2n}}}{\displaystyle\sum_{n=1}^{\infty} \frac{\nu^{(n+1)}}{(n+1)!}} \\
&= 2\frac{\rho}{r^2} \frac{\left[\left(1 - \frac{\rho^2}{r^2}\right)\nu - 1\right]e^{(1-\frac{\rho^2}{r^2})\nu} + 1}{(e^\nu - 1 - \nu)\left(1 - \frac{\rho^2}{r^2}\right)^2} \\
&\approx C\,\rho\exp\left(-\pi\beta\rho^2\right)
\end{aligned} \tag{F.6}
$$

for $\rho \in [0, \delta]$, where C is the appropriate normalizing constant. In the last step in the above equation, we have used approximations based on assumptions $\nu \gg 1$ and $r \gg \delta$. Figure F-1 shows the probability density function $q(\cdot)$ for several different values for β.

It follows from the two-object merging model, p_m, defined by (4.6), and (F.2) to (F.6) that

$$
\begin{aligned}
P_M &\approx \int_0^\delta p_m(\rho)q(\rho)d\rho \\
&\approx 2\pi\beta\left[\int_0^{\delta/2} \rho e^{-\pi\beta\rho^2}d\rho + 2\int_{\delta/2}^\delta \frac{\delta - \rho}{\delta}\rho e^{-\pi\beta\rho^2}d\rho\right] \\
&= 1 - \frac{2}{\delta\sqrt{\beta}}\left[\text{erf}\left(\sqrt{2\pi\beta}\delta\right) - \text{erf}\left(\sqrt{2\pi\beta}\frac{\delta}{2}\right)\right]
\end{aligned} \tag{F.7}
$$

which proves (4.8).

We should note here that the probability of measurement merging (or unresolved measurements), P_M, is a function of the object density β, or the object density normalized by
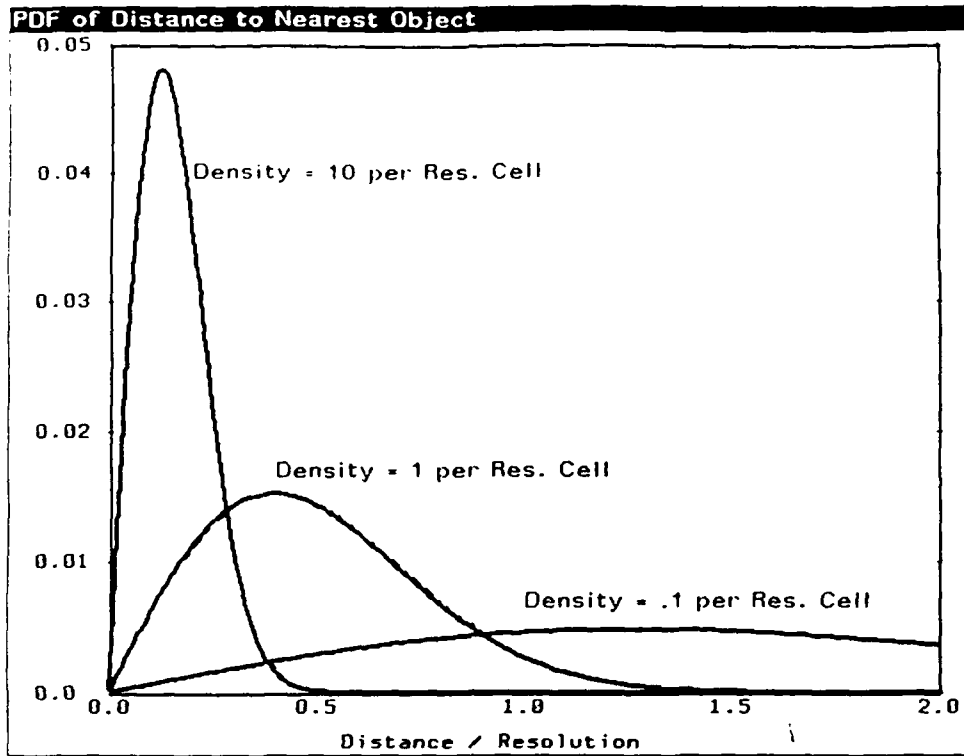
PDF of Distance to Nearest Object

Figure F-1: Probability Density Function of Distance to Nearest Object

the sensor resolution, i.e., $\beta\delta^2$. As expected, we have $P_M \uparrow 1$ as $\beta\delta^2 \uparrow \infty$ and $P_M \downarrow 0$ as $\beta\delta^2 \downarrow 0$. We have assumed the object density β to be uniform. If the density is not uniform (as discussed in Appendix C), the calculation of the probability density functions, (F.5) and (F.6), may become very complicated, and hence, we may not have a concise expression such as (4.8). However, if the change of the object density is *gradual* enough relative to the sensor resolution δ, the probability P_M may be accurate when β is replaced by the local object density, and the overall (average) probability may be given by appropriate integration.

REPORT DOCUMENTATION PAGE

1a. REPORT SECURITY CLASSIFICATION Unclassified			1b. RESTRICTIVE MARKINGS			
2a. SECURITY CLASSIFICATION AUTHORITY			3. DISTRIBUTION/AVAILABILITY OF REPORT Approved for public release; distribution is unlimited.			
2b. DECLASSIFICATION/DOWNGRADING SCHEDULE						
4. PERFORMING ORGANIZATION REPORT NUMBER(S) ADS-TR-1196-1			5. MONITORING ORGANIZATION REPORT NUMBER(S) ESD-TR-89-128			
6a. NAME OF PERFORMING ORGANIZATION Advanced Decision Systems	6b. OFFICE SYMBOL (If applicable)		7a. NAME OF MONITORING ORGANIZATION Electronic Systems Division			
6c. ADDRESS (City, State, and Zip Code) 1500 Plymouth Street Mountain View, CA 94043-1230			7b. ADDRESS (City, State, and Zip Code) Hanscom AFB, MA 01731			
8a. NAME OF FUNDING/SPONSORING ORGANIZATION Lincoln Laboratory, MIT	8b. OFFICE SYMBOL (If applicable)		9. PROCUREMENT INSTRUMENT IDENTIFICATION NUMBER BX2202			
8c. ADDRESS (City, State, and Zip Code) P.O. Box 73 Lexington, MA 02173-0073			10. SOURCE OF FUNDING NUMBERS			
			PROGRAM ELEMENT NO.	PROJECT NO. 359-03-201	TASK NO.	WORK UNIT ACCESSION NO.

11. TITLE (Include Security Classification)

Tracking Performance Evaluation

12. PERSONAL AUTHOR(S)
Shozo Mori, Kuo-Chu Chang, Chee-Yee Chong, and Steve Spain

13a. TYPE OF REPORT Final Report	13b. TIME COVERED FROM 12/1/87 TO 8/31/88	14. DATE OF REPORT (Year, Month, Day) 1988, December 7	15. PAGE COUNT 76

16. SUPPLEMENTARY NOTATION

None

17.	COSATI CODES		18. SUBJECT TERMS (Continue on reverse if necessary and identify by block number)
FIELD	GROUP	SUB-GROUP	multitarget multisensor tracking, SDI tracking, midcourse tracking, ballistic missile defense systems, track purity, performance evaluation, track-measurement association, track accuracy, performance prediction, (correlation), object density, closely spaced objects

19. ABSTRACT (Continue on reverse if necessary and identify by block number)

This final report documents the research conducted at Advanced Decision Systems, sponsored by Lincoln Laboratory, Massachusetts Institute of Technology, under a project entitled, "Discrimination Architecture Engineering Support," from 1 December 1987 to 31 August 1988. In this research, simple analytic models were developed for predicting performance of tracking systems in terms of track purity under given tracking environments, in particular, multilayer ballistic missile defense environments concerning tracking-surveillance and object-discrimination. The main result is a simple analytic model which relates single-scan track-to-measurement association (correlation) performance to two key parameters, object density on sensors' focal planes, and average measurement prediction accuracy by tracks. Predicted track purity is then calculated, through this model, based on given object trajectories and sensor deployment patterns. Extended models were developed to account for false alarms and merged measurements (CSOs) due to limited sensor resolution. Small-scaled but fairly extensive Monte Carlo simulations support the analytic models for predicting track purity developed through this project.

20. DISTRIBUTION/AVAILABILITY OF ABSTRACT ☐ UNCLASSIFIED/UNLIMITED ☒ SAME AS RPT. ☐ DTIC USERS	21. ABSTRACT SECURITY CLASSIFICATION Unclassified	
22a. NAME OF RESPONSIBLE INDIVIDUAL Lt. Col. Hugh L. Southall, USAF	22b. TELEPHONE (Include Area Code) (617) 981-2330	22c. OFFICE SYMBOL ESD/TML

DD FORM 1473, 84 MAR · 83 APR edition may be used until exhausted. · All other editions are obsolete.